CHALMERS

Effect of diffusion bonded Cu and Ni on sinter hardening response of Mo prealloyed PM steel

Seshendra Karamchedu

Department of Materials and Manufacturing Technology

Supervisor: Sepehr Hatami
Examiner: Prof. Lars Nyborg

Abstract

Through utilization of hardenable powder in combination with accelerated post sintering cooling rates, sinter hardening offers good manufacturing economy as well as unique combination of mechanical properties. In order to obtain desired mechanical properties, the microstructure can be manipulated to form the required amount of martensite and bainite using suitable alloying system.

The aim of the current study is to outline the sinter hardening response of Astaloy Mo based PM steels. For this purpose and to elucidate the effect of the alloying, together with Astaloy Mo (prealloyed with 1.5% Mo), Distaloy DH (diffusion bonded with 2 wt. % Cu) and Distaloy DC (diffusion bonded with 2 wt. % Ni) were examined.

For each alloy tensile samples were manufactured by sintering at 1120°C for 30 minutes and cooling at a rate of 2.5 °C/s (within 800 to 300 °C). Afterwards, the tensile specimens were subjected to a tempering treatment at 200 °C for 60 minutes. Distaloy DH and Distaloy DC with two different levels of admixed graphite content (i.e. 0.55 and 0.7 wt. %), and Astaloy Mo admixed with 0.55 wt. %C have been investigated for tensile properties, hardness, microhardness, porosity and residual stresses. Metallographic examination using optical microscopy along with scanning electron microscopy (SEM) combined with energy dispersive X-ray analysis (EDX) has been performed in an attempt to relate the results obtained from the mechanical testing to the microstructure of the alloys.

Regarding tensile properties, Distaloy DH was seen to be slightly better than Distaloy DC while Astaloy Mo possessed the lowest values. Increase in graphite content did not contribute to a significant increase in tensile strength; however, it resulted in a decrease in elongation for both Distaloy DC and Distaloy DH. These findings were related to the fully bainitic microstructure of Astaloy Mo as compared to a bainitic-martensitic microstructure of Distaloy materials. A correlation between the microhardness and the effect of distribution of alloying elements has been proposed, with which the microstructure development can be explained. Regarding surface residual stresses, Astaloy Mo had a compressive surface stress state, while for the other materials it was tensile but with very low values. For all the materials analyzed, porosity analysis revealed that, for a particular size range or pores their shape was similar.

In conclusion, the investigation presents a comparative study on the effect of addition of 2 wt. % Cu and Ni (to Astaloy Mo) on the microstructure and the resulting influence on the final mechanical properties.

Acknowledgement

I would like to start by thanking my examiner Prof. Lars Nyborg and my supervisor Sepehr Hatami for extending their unconditional support and guidance all along my thesis work.

I wish to thank Höganäs AB (Höganäs-Sweden) and Dr. Michael Andersson for providing the materials to carry out this thesis work and their technical support

My thanks are due to Prof. Maria Knutson Wedel for acting as my program coordinator. I also express my sense of gratitude to Dr. Peter Sotkofsky and Dr.Kenneth Hamberg for giving me invaluable suggestions in completing my work and for their help with metallography. I would like to thank Dr. Yao Yiming for helping me in carrying out the SEM investigations. I would like to extend my thanks to thank Mr. Urban Jelvestam for assistance with sample preparation.

I would thank all the faculty members of the Department of Materials and Manufacturing Technology and my classmates who have supported me throughout my stay at Chalmers.

Finally, I would like to thank my parents, teachers and friends in India who have been a constant source of encouragement.

Table of Contents

List of Figures

1. INTRODUCTION

1.1 Background

Sinter hardening is a manufacturing route used for powder metallurgy alloys that can transform to the hard martensite phase upon cooling from sintering temperature. PM structural parts must of course have adequate mechanical properties for the intended application, however, their lower final cost is the main reason for fabricating them from powder [1].The technique of sinter hardening is proven cost effective since it eliminates the need for post sintering heat treatment. It is used in applications requiring high strength and hardness.

For the purpose of sinter hardening, certain powder grades are formulated which have higher hardenability than conventional PM steels. Alloying elements, depending on the method employed to introduce them into the base iron powder, can influence compressibility and sintering behavior. For the case of prealloyed powders, compressibility is suffered but homogenous microstructure is attained. However, when the alloying elements are introduced by diffusion bonding, compressibility is retained but a heterogeneous microstructure is inevitable. Solid solution strengthening effect caused by Mo is lower among the familiar additions, which implies that the compressibility retention upon alloying Mo is high. This is one of the choice criteria in the introduction of Astaloy Mo [2]. Traditional sinter hardening alloys contain low alloy iron powders mixed with Cu, Ni and carbon [3]. To optimize manufacturing costs and performance of sinter hardened parts, the choice of alloying elements, their content, and the method of alloying has to be tailored.

In the current study, an attempt is made to understand the influence of alloying system on the sinterhardening response. For this purpose, Astaloy Mo and its diffusion bonded derivatives, that is, Distaloy DH (Astaloy Mo with 2wt.% of diffusion bonded Cu) and Distaloy DC (Astaloy Mo with 2wt.% diffusion bonded Ni) have been chosen for investigation.

1.2 Scope and Objective

The present study is concerned with the following alloying systems:

1. Astaloy Mo (Water atomized Fe powder prealloyed with 1.5 wt.% Mo)
2. Distaloy DC (Astaloy Mo diffusion bonded with 2 wt%. Ni)
3. Distaloy DH (Astaloy Mo diffusion bonded with 2 wt%. Cu)

The Distaloy materials with two variants in admixed graphite i.e., 0.55 wt. % and 0.7 wt. % and Astaloy Mo with 0.55 wt% were chosen for this study.

The work aims at elucidating the effect of Cu, Ni and graphite on the response of these alloys to sinter hardening. A literature study was carried out and the effects of individual alloying elements on various aspects of PM steels were gathered. Experimental work has been undertaken on the above mentioned alloys, and their mechanical properties were investigated. In addition, microstructural characterization of the alloys was conducted using optical and scanning electron microscopy. Furthermore, surface residual stress measurements were performed on all samples. The focus of the current work is on the effect of

alloying elements, and it does not deal with other factors which influence the sinterhardening behavior such as the cooling rate, density, porosity and sintering conditions.

The objective of the current work is to:

- Perform mechanical testing and hardness testing for the materials chosen to understand their mechanical behavior.
- Carry out metallographic investigation to study the influence of microstructure on the obtained mechanical properties.
- Evaluate the surface residual stresses of the alloys and obtain a relationship between the microstructure and these stresses.
- Investigate the effect of diffusion bonded alloying elements on evolution of microstructure by thorough SEM and EDX studies.
- Perform porosity analysis on the individual alloys and relate the results to the effect of alloying.
- Evaluate the usefulness of the induced property changes by each of the included alloying elements.

2. LITERATURE SURVEY

2.1 Introduction to Sinter Hardening and Hardenability of Powder Metallurgy Steels

More high performance components requiring heat treatment are now being processed using Powder Metallurgy (PM) route, owing to its cost effectiveness and near-net shape capability [4]. While it is the improvement in processing methods and development of new materials that contributed significantly to the growth of the same, sinter hardening is a process that has emerged on these lines. In this process the post sintering cooling rate employed is fast enough so that a significant portion of the material matrix is transformed into martensite. Hence, it presents cost effectiveness as the secondary quench and tempering treatment is avoided. When compared with quench and tempering process, sinter hardening is advantageous since the problem of retention of quenching oil is eliminated. Furthermore, components experience less severe quenching in sinter hardening (as compared to oil quenching) which offers better dimensional control [4,5].

Martensite which is the hardest transformation constituent in steels is an important microconstituent, since achieving high strength and hardness is often the main goal of sinter hardening. Hence, the ability of a material to promote martensitic transformation during the cooling cycle after sintering becomes the governing factor. The phase transformation processes that form the basis for heat treatment of steels have been thoroughly studied for the case of wrought steels [4]. The depth and distribution of hardness for steel is qualitatively measured as hardenability, which is at the same time indicative of the ability of steel to transform to martensite. For wrought steels, hardenability is dependent on the chemical composition and austenite grain size.

While the heat treatment process for PM parts can be the same as that for wrought steels and the knowledge from heat treatment of wrought steels can be informative, PM steels are still quite different. The difference arises mainly because the transformation response to heat treatment is also influenced by porosity and compositional inhomogeneity. It should also be considered that there are many PM compositions for which there exist no wrought analogs and thus, the knowledge of the specific system is necessary for proper heat treatment [5].

If the alloy system offers sufficient hardenability, relatively larger parts can be sinterhardened without the need for accelerated cooling. Rapid cooling allows the usage of leaner alloy grades. Proper material selection and an understanding of hardenability would avoid over-engineering, enabling an economic choice of material and process for the application [6]. For sinterhardened parts, the sintering process provides austenization treatment necessary for the steel compacts. These steels should possess high hardenability to allow sufficient depth of martensite formation at relatively slow cooling rates which are possible in the sintering furnace. However, high apparent hardness and strength achieved immediately after sintering makes sizing and other secondary operations impractical [5].

2.1.1 Quench and Tempering

Traditional heat treatment of PM parts has the quench and tempering stage as a separate step in processing. The properties achieved after quench and tempering treatment depend on severity of

quench attained by the cooling medium and on the hardenability of the PM steel. Though higher heat transfer rates leading to faster quench can be achieved using water, brine or water-based polymer solution, oil quenching is favored for PM steels. The reason being, the residual quenchant in the case of quenching media other than oil accelerates the corrosion in the parts. Also oil quenching offers minimized distortion and cracking. The oil temperature and its characteristics can furthermore be adjusted to improve the heat transfer. [4]

Tempering reduces the effects of retained austenite formed in the low alloy steels when rapidly quenched. PM parts can however absorb nearly 2 to 3 wt% oil which cannot be disregarded while considering post quench treatment. Incomplete removal of oil during tempering can result in heavy smoke which is hazardous to health and also poses safety concerns when present in large amounts in the tempering furnace. The recommended tempering temperatures for PM parts range from 150 to 200°C, tempering above this range improves toughness and fatigue performance but on the other hand compromises tensile strength and impact resistance. Care should also be taken as the entrapped oil can ignite when tempered above 200°C. [4, 5]

The final microstructure determining the properties of heat treated sintered parts depends on several factors including particle size, density, composition, homogeneity of alloying distribution, sintering temperate and time, cooling rate and the subsequent tempering treatment [5]. For a given iron based powder and heat treatment conditions, the microstructure and properties depend upon the alloying elements and the method of alloying. It can be summarized that an understanding of the effect of alloying elements, compositional inhomogeneity, porosity in the material and the process parameters is necessary to anticipate and evaluate the microstructural development.

2.2 General Aspects of Alloying in PM Steels

This section presents and overview of the effect of individual alloying elements with respect to their contribution to mechanical properties and microstructure for sintered parts. Focus is on those alloying elements that are relevant for the experimental work of this thesis.

2.2.1 Carbon

For wrought steels, the tensile strength and hardness levels increase proportionally with increasing carbon content up to 1.2 wt. % [5]. However, in the case of PM steels, generally, the maximum strength is reached at eutectoid composition in the as sintered condition [5]. Alloying content exceeding eutectoid composition will result in the formation of carbide network along the porosity channels and grain boundaries, resulting in embrittlement and loss in strength. However, for carbon steels, in the hardened and tempered condition peak strength is obtained at 0.65%C [5]. The optimum carbon level decreases with the addition of alloying elements. Though addition of carbon is an efficient way to improve properties, successful sintering of carbon containing materials requires a very carefully controlled non-decarburizing sintering atmosphere [7].

2.2.2 Copper

Cu increases both apparent hardness and tensile strength in the as sintered condition. However, subjected to hardening treatment, it contributes to an increase in hardness at the expense of loss of

toughness and strength. The rupture strength rises to an optimum level with the increase in copper content and then declines. Unlike progressive softening upon tempering which is the case for Fe-C steels, the Fe-C-Cu steels show significant temper resistance up to 371°C. It was also observed that the heat treated strength overlaps with sintered strength and optimal properties for these alloys upon heat treatment were obtained at 2 wt. %Cu [5]. Copper is added usually between 1.5-4 wt. %; and when steel is alloyed with more than 2.5wt. % Cu, dimensional tolerances are difficult to control. This is due to the growth that copper promotes during sintering and a suitable amount of graphite has to be added to control this effect. This will be discussed in the dimensional changes section in detail. Further, the solubility of Cu in ferrite is only 0.4% while the austenite can dissolve 9%Cu, consequently the Fe-Cu alloys can be precipitation hardened by low temperature annealing after sintering [4,7].

2.2.3 Nickel

Nickel contributes to an increase in tensile properties of as-sintered parts but to an extent lower than the case for Cu [5]. Upon heat treatment, it contributes to a significant improvement in mechanical properties. Cu melts at 1083°C and hence during sintering, which is usually performed at 1120°C, it results in a more homogenous structure. This is as opposed to case of nickel which has a higher melting point (1453°C) than the sintering temperature, it combines with iron only through solid state diffusion which results in nickel rich islands and partially alloyed regions [8]. When quenched, the islands remain austenitic resulting in the duplex microstructure which will be discussed later under the effect of starting material on homogenization section.

2.2.4 Chromium

It is a ferrite stabilizer and increases the hardenability and significantly improves the mechanical properties even when added in small amounts. It has the lowest effect on compressibility [9] due to its low solid solution strengthening effects and is less expensive than the more common alloying elements. When it replaces the nobler elements like Ni, it results in an overall lowering in alloy content owing to its effective alloying. The shortcoming for alloying Cr is its high affinity towards oxygen which restricted its use. However, by prealloying Cr into the base iron powder, oxidation problems were eliminated to a large extent.

2.2.5 Copper and Nickel

It was noticed that when Jominy tests were performed on bars pressed to 6.7 g/cc density with a fixed carbon content (0.5 wt. %) and increasing amounts of copper and nickel [4]:

- An increase in copper content to 2.5 wt.% resulted in dramatic increase in the surface hardness but the depth of hardening was not significantly improved
- With the addition of nickel there was a small increase in the surface hardness but the depth of hardness increased significantly.

Adding Ni to Fe-C or Fe-Cu-C alloys has an effect similar to that of addition of Cu. However, replacement of Cu by Ni renders a better dimensional control during sintering. In addition, it has been reported that Ni-rich austenite phases can enhance elongation in some cases [7].

2.2.6 Molybdenum

Molybdenum is more effective than nickel for enhancing hardenability. Molybdenum additions are usually in the range of 0.5 to 1.5% to promote heat treatment response, increase in hardness, wear resistance and strength to the required level in highly loaded PM parts. Molybdenum has lower affinity for oxygen and lower effect on compressibility when compared to nickel. [5]

2.2.7 Molybdenum, Nickel and Copper

For alloys with molybdenum, nickel and copper, at a fixed carbon and molybdenum content of 0.5 wt%, an increase in hardness and significant increase in tensile strength was noticed when the nickel and copper contents were increased to 4% and 2.25% respectively. Also the ductility improved at all cooling rates with an increase in Cu and Ni content. The alloy with the highest additions in nickel had the lowest dimensional change at all cooling rates and thus, it is expected to result in lower residual stresses. [5]

2.2.8 Effect of Alloying Elements on Martensitic Transformation

The efficiency of alloying elements with respect to their contribution to hardenability is as follows: Mn>Cr>Mo>Cu>Ni [10,11], Mn being most effective and Ni having the least influence. The minimum cooling rate required for the martensite formation depends upon the composition of steel. This in turn controls the temperatures and rates at which the non-martensitic products form and has been studied extensively. The diffusion less transformation of martensite starts at a temperature designated by M_s and continues until a martensitic finish temperature M_f. The M_s in steels depends upon a) the equilibrium temperature between austenite and ferrite b) strength of austenite [12]. Both these factors are affected by the alloying elements and this can be shown by an empirical relationship stated by equation 1

$$Ms\ (°C) = 520 – 320\ (\%C) – 50\ (\%Mn) - 30(\%Cr) - 20(\%(\ Ni+Mo)) - 5(\%(\ Cu+Si)) \quad \text{Eq. 1} \quad [5]$$

Several empirical equations have been proposed over the years by several authors. Andrews developed these equations based on measurements of M_s temperatures for large number of steels. It was observed that 92 to 95% of the measured values lied within ±25°C of the temperatures calculated, see equation 2 and equation 3. (13) [13]

$$Ms\ (°C) = 539 – 423\ C – 30.4\ Mn – 12.1\ Cr – 17.7\ Ni – 7.5\ Mo \quad \text{Eq.2} \quad [13]$$

$$Ms\ (°C) = 512–453C–16.9Ni–15Cr– 9.5Mo + 217(C)^2 – 71.5(C)(Mn) -67.6\ (C)(Cr) \quad \text{Eq.3} \quad [13]$$

The element symbols in the formula correspond to weight percentages of the elements. The calculations from this formula for steels containing 0.2-0.8%C are in good agreement with the experimental data (5)[5]. However, for multialloy steels it does not always yield reliable data since the interaction effects cannot be represented by simple summation. The M_s is affected mostly by the dissolved carbon in austenite and the M_f decreases significantly as the carbon content increases up to 1% and remains constant at higher amounts of carbon. [14]

Characteristic feature of martensitic transformation in steels is that the austenite to martensite transformation is never complete. The transformation starts at M_s and the amount of martensite increases with decrease in temperature up to M_f at the end of which certain amount of retained

austenite is left. If the martensite finish temperature is below room temperature, the amount of retained austenite should be higher the lower the M_s temperature. [4,14]

2.3 Effect of Starting Material on Homogenization

The most important function of alloying elements in heat treatable steels is to increase hardenability. The choice of alloying elements for sintered steels is influenced by factors different from those for wrought steels. One such factor is that the green compact presents extremely high surface area to the atmosphere and hence there is a higher risk for oxidation than in the case of solid material. It is for this reason that noble metals like Cu, Mo and Ni are used in spite of their higher cost in PM steels. [15]

Sintering atmosphere with low oxygen partial pressures plays an important role in sintering of Cr alloyed steel powder. Elements like Cr have high oxygen affinity and hence have a strong tendency towards forming thermodynamically stable oxides during powder production [16]. For such elements prealloying is commonly used. When prealloyed, these elements are present in solid solution which lowers their activity [16].

There can be different types of powders used as the starting material for PM steels. The alloying method affects the microstructural development and the final mechanical properties. The four different powders used are **admixed, diffusion alloyed, prealloyed and hybrid powders**. For the case of admixed powders, the compressibility is high but the degree of alloying is limited by the mutual diffusivity of the elements added. Admixed powders suffer from segregation during handling and exhibits high microstructural heterogeneity. Diffusion bonded powders show heterogeneous microstructures with an alloying gradient between the centre of former powder particles and highly alloyed interparticle boundaries. The problem of segregation during handling is avoided and high compressibility is retained. In the case of prealloyed powders all alloying elements except carbon are added to the melt. The powder is produced by atomizing the melt. The microstructure of prealloyed powder is homogeneous; however, prealloyed powder have lower compressibility than that of admixed and diffusion bonded. [2,17]

Hybrid alloys with molybdenum prealloyed have master alloy additions to create new series of hybrid alloys, they possess less homogenous microstructure but the compressibility is retained. [2]

Alloying additions affect sintering behavior and compressibility of the powder. In prealloyed condition, among Si, Mn and Cr, silicon has the worst influence on compressibility. In the case of more familiar additions, it is stated that both Mo and Ni when dissolved into iron bring about hardness increase but hardening effect caused by Mo is lower than that of Ni. The influence of different alloying elements on the compressibility is illustrated in *Figure 1* [18]. From figure 1 it can be seen that for a composition similar to Astaloy Mo (Fe-1.5Mo wt. %) compressibility decrease is about 1.5% of that for a pure iron grade.

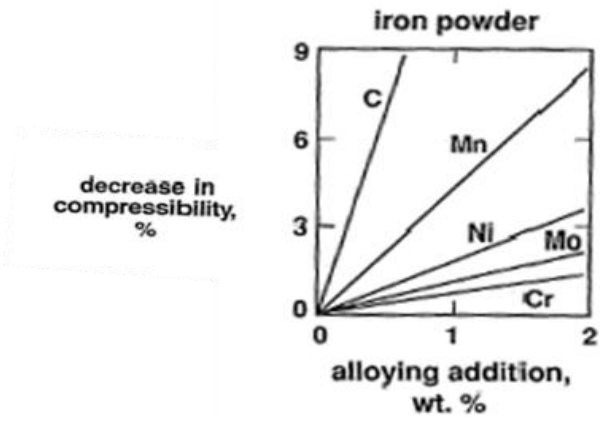

Figure 1 Decrease in compressibility Vs concentration of prealloying ingredients added to water atomized iron powder [18]

Carbon, typically added in the form of graphite powder has high diffusion at sintering temperatures resulting in homogenous distribution when no other alloying elements are present. However, it has been observed that carbon can affect the diffusion of some alloying elements. When powders admixed with graphite and copper are used, it is shown that at higher carbon contents the diffusion of copper is inhibited. The carbon diffused in the austenite, promotes the formation of retained austenite at the particle/pore surfaces. However, it is considered that the level of retained austenite thus obtained did not interfere with the part performance in commercial practice. [19]

As stated earlier the Ni addition results in a greater degree of inhomogeneity. This is due to its lower diffusion coefficient as compared to Mo [17] and Cr [13] in austenite. More rapid homogenization is observed in the case of alloying elements which form solid solutions which are body-centered cubic such as with Cr, Mo and Si. This is because, for the case of elements in which ferritic alloys are formed, the diffusivity is two orders of magnitude higher than the case when austenitic solid solutions are formed, like in the case of Fe-Ni and Fe-Mn [1]. Also, between 900 and 950°C the diffusivity of Ni is only 1% of its rate at conventional sintering temperatures. At sintering temperatures, a rise in temperature from 1100 to 1150°C increases the diffusivity by twofold. Hence, 25°C of variation in temperature can cause a 50% difference in nickel diffusion rate [5]. The temperature uniformity is thus a determining factor for alloy distribution. Furthermore, if the local concentration of Ni exceeds a certain limit austenite will be stabilized regardless of the cooling rate. This austenite should be clearly differentiated with retained or residual austenite since it is stable or incoercible. These randomly distributed areas of soft austenite can contribute to resistance to stresses by means of local plastic-yielding. However, for the case where much lower amounts of austenite is not distributed finely, the influence instead is detrimental, when lower amounts of austenite is present and not dispersed finely [20].

Apart from the low diffusivity of Ni, the repulsion effect between Ni and C is considered to be a factor contributing to microstructure inhomogeneity leading to the presence of Ni-rich ferrite or austenite. It is reported that addition of Mo or Cr would decrease the chemical potential of carbon in the Ni-rich areas and enhance the alloy homogenization. Lowering of the carbon chemical potential by Cr and Mo is attributed to their strong carbide forming ability. [21]

In an Investigation the effect of Cu, Ni, Mo and graphite addition to base iron powder by different alloying methods on the mechanical behavior was studied. It was inferred that the addition of Mo by diffusion bonding increased the tensile strength significantly than when it was admixed or prealloyed. Prealloying Mo resulted in yield strength exceeding its diffusion bonded counterpart but the tensile strengths and impact energies were comparable. It was also observed that the prealloyed Mo material had half the level of elongation in comparison with the case where it is diffusion bonded. With regard to Cu, the size of Cu powder did not cause any significant change in the yield strength but the tensile strength was improved with smaller particle size. Furthermore, it is known that coarser copper powder promotes inhomogeneity and is detrimental to ductility. The work suggested that the prealloyed Mo powder was more sensitive to parameters with respect to dimensional change than when it was diffusion bonded [22].

2.4 Dimensional changes

Dimensional precision is a key attribute in the manufacturing of net shape parts. Dimensional control of sinter hardening alloys is more challenging than traditional materials as the martensite formation results in more growth than other phases. While tempering can be used to reduce this growth, the presence of retained austenite in heavily alloyed regions reduces the overall growth of the sintered compacts. Separately, elemental additives such as Cu and graphite to the powder cause growth and Ni causes shrinkage. [7,23]

Base iron composition and cooling rate have a pronounced effect on the microstructure. The high temperature phase in steel, austenite transforms to (i) ferrite and carbide to form pearlite or bainite (ii) martensite, or a combination thereof. In addition to this, this austenite can remain in the heavily alloyed regions (retained austenite). Austenite is the highest density phase in steel, followed by ferrite and carbide and finally martensite, which is the lowest density phase in steel. Length changes in fully dense materials can reach 1.4% upon transformation from austenite to martensite [24].When tempered, the martensite transforms into a ferrite and carbide structure which has a higher density and hence decreasing the dimensional change of the martensitic sintered compact.

Dimensional changes in compacts are not only dependent upon the powder characteristics but also upon a large number of other factors such as green density, heat-up rate, sintering time, sintering temperature, cooling rate, sintering atmosphere and the type of furnace. [1]

2.4.1 Carbon

At common sintering temperatures (e.g. 1120C), graphite quickly goes into austenite. Dilatometric studies have shown that this solutionizing cause growth beyond that associated with thermal expansion of iron. The dimensional change (shrinkage) that occurs at the sintering temperature is smaller than the carbon solutionizing growth. As the carbon remains in the steel on cooling in the form of carbide or in solution in martensite, the sample retains growth. This growth increases with the amount of graphite. [20]

2.4.2 Copper and Carbon

In compacts made from iron copper powder mixture, upon sintering, the copper penetrates into the interstices between particles and into grain boundaries upon melting. Thereby it results in an effect of wedging them apart and contributing majorly to expansion. In addition, the diffusion of copper into iron causes growth. [1]

It has been observed that growth occurs in Fe-Cu alloys at 1083°C which is the melting point of Cu (peritectic temperature in the iron-copper system being 1094°C [1]). This growth was significantly reduced in the high carbon alloys. Increase in carbon content increases the wetting angle and dihedral angle of liquid copper on iron. Consequently, retardation of the flow of Cu along the particle surfaces and into grain boundaries results in lower amount of growth. Therefore, dimensional change in high carbon high copper mix can be less than if either additive were made alone [19]. When the same amount of Cu was prealloyed to the material, it behaves like pure iron base with no admixed copper with respect to dimensional change. This is because the wetting and dihedral angle change due to the effect of carbon would be irrelevant for this case.

It is found that increase in carbon content has little effect when the amount of Cu is up to 1 wt. % since the interaction effect is not very significant. However, for most sinter hardening applications, alloys with 2 wt. % Cu are generally used in which case the increase in C reduces the dimensional change. Previous research has shown that the amount of retained austenite can be used as a parameter to control the dimensional change to a small degree in compositions having higher hardenability. Dimensional control can also be brought about through usage of iron powder particles which are highly porous, so that the copper is absorbed upon melting into the porous structure of the particles rather than penetrating between particles. [1,19,25]

2.4.3 Dimensional control in Cu-Ni containing ferrous PM alloys in prealloyed Mo based materials

The effect of Mo and C with varying Cu contents can be read from *Figure 2*. As illustrated in Figure 2 the effect of Cu and graphite is in accordance with the previous discussion. Changing the content of Mo, from 0.3 wt. % to 0.8 wt. % slightly lowers the dimensional change. The reasons were not fully understood and it was mentioned that this slight change could be due to the base alloy particle distribution. When this system was alloyed with 2 wt. % Ni, the effect of Mo or different base alloy particle size was no longer evident. Also, the effect of carbon content on the dimensional change was virtually eliminated. The nickel containing and Ni free samples were cooled at different rates to achieve similar microstructure and hardness; nevertheless, they resulted in different dimensional changes. It was stated that transformation products were not the only reason for dimensional change in this regard. It was speculated that there exists an interaction between Cu and Ni in a way that the Cu tends to diffuse to Ni-rich regions, causing this behavior. Also the dimensional change is directly related to the size of the Cu powder; smaller the powder, lesser the growth. [20]

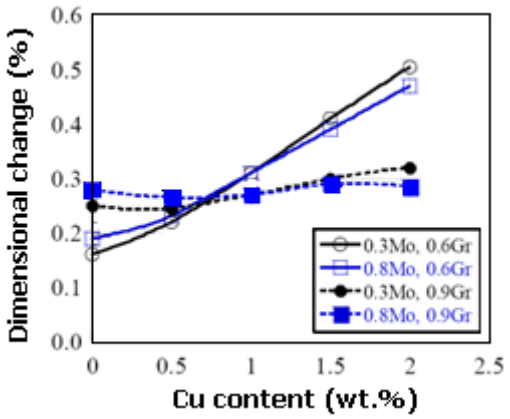

Figure 2 Effect of Mo and C on dimensional change with variation in Cu content [25]

2.5 Astaloy Mo Based Powders

Astaloy Mo is a water atomized powder prealloyed with 1.5 wt. % Mo which exhibits high compressibility and a homogenous microstructure. Prealloyed Mo along with 0.2 to 0.6 wt. % admixed graphite promotes hardenability, making it an excellent choice for parts requiring high surface hardness and good core toughness [26]. It is known that alloying Mo shifts the eutectoid compositions to lower carbon contents, and contracts the austenite phase field by shifting the A_{CM} boundary to higher temperatures for a given carbon content. It has also been found that the austenitizing temperature of 845°C was insufficient to completely austenitize the systems with Mo content and carbon (Mo>0.5wt. %). [27]

Beneficial effects of Cu and Ni additions and the possibilities of hybrid powders based on Astaloy Mo have been mentioned earlier. Two hybrid alloys based on Astaloy Mo and containing Cu and Ni are Distaloy DH and Distaloy DC respectively. **Distaloy DC** contains 2 wt. % Ni and 1.5 wt. %Mo and is produced by diffusion bonding of Ni powder to Astaloy Mo. It exhibits little dimensional scatter for components with intricate shapes. With admixed graphite this material offers high strength after sintering [28]. The nickel content can form retained austenite in the microstructure. **Distaloy DH** contains 2 wt. %C and 1.5 wt. %Mo and is produced by diffusion bonding 2 wt. %C to Astaloy Mo. When admixed with graphite it transforms into a very hard martensitic-bainitic microstructure with high tensile strength values when cooled from sintering temperature at cooling rates of 4-8°C/s. [28]

In terms of mechanical performance in applications requiring high strength Distaloy DH or a hybrid powder with Astaloy Mo base with a minimum of 1.5%Cu is suggested. However, Distaloy DH is notch sensitive. On the other hand, for application requiring high impact strength with low notch sensitivity hybrid powders of Astaloy Mo diffusion bonded with Ni close to 4 wt. % is suggested as the best choice [26].

2.6.1 Dimensional Changes

- Swelling was observed during sintering of Distaloy DH and the dimensional change was lower when using 0.65 wt. % admixed graphite as compared to 0.8wt. % [11]. An increase in dimensional change with increase in cooling rate for particular carbon content (give carbon content) was reported (give reference) .The author reports in (give the reference) that the

cooling rate did not have any influence on the dimensional changes for both Distaloy DH and Distaloy DC [29].

2.6.3 Yield Strength and Tensile Strength

- It was reported in [11] that for Distaloy DH at lower carbon level (0.65 wt. %), the yield strength and tensile strength increased with increase in cooling rate and density. At higher carbon level (0.8 wt. %), both the yield strength and the tensile strength were reported to be either equal to or lower than the values obtained at the lower carbon level. This trend was seen at both the density levels (6.9 and 7.0 g/cc). It was stated as an explanation that with increased carbon, martensite becomes more fragile which resulted in an increase in hardness but decrease in the mechanical properties.
- The trends for the yield strength of Distaloy DH reported in [29] were in agreement with those discussed in [11]. Distaloy DC also followed similar trend. However, the increase in yield strength with increasing cooling rate was higher for Distaloy DC (24%) than that for Distaloy DH (19%). At lower cooling rate (2 °C/s) Distaloy DH had higher yield strength than Distaloy DC but at higher cooling rate (5-6 °C/s); the yield strength was reported to be similar for both. By increasing the cooling rate the tensile strength increased by 20% for Distaloy DC whereas For Distaloy DH only a 5%increase in the tensile strength was observed2.6.4 Microstructural Response
- With the CCT curves constructed from the metallographic investigation in [11], Figure 3, it could be deduced that at 2.5°C/s the microstructure of Distaloy DH with 0.65 wt.% of admixed graphite consisted of 30% bainite and 70% martensite. While for 0.8 wt. %C, the microstructure was 90% martensite and 10% bainite. The microstructure of Distaloy DH was sensitive to increase in cooling rate which was reflected in an increase in hardness, yield strength and tensile strength. It was also inferred from the results that for Distaloy DH with 0.8wt. %C a cooling rate greater than or equal to 2.5°C/s is necessary to obtain 90% martensite in the microstructure
- According to [29] it was reported that with 0.7 wt.% of admixed graphite at a cooling rate of 10Hz (2 °C/s) Distaloy DC has 75 vol.% bainite and 25 vol.% martensite whereas, Distaloy DH has 40 vol.% bainite and 60 vol.% martensite. When cooled at a rate of 60Hz(5-6°C/s), the microstructure of Distaloy DC consisted of 1 vol. % bainite and 99 % martensite whereas for Distaloy DH the microstructure was fully martensitic *Figure 4*,. Density did not influence the microstructural response in the case of these alloys for conditions examined in this work. The results obtained are however different from those obtained in [11].
- The microstructural investigation of Distaloy DC, DH at both density levels and at both cooling rates tested according to [29] are tabulated Table 1

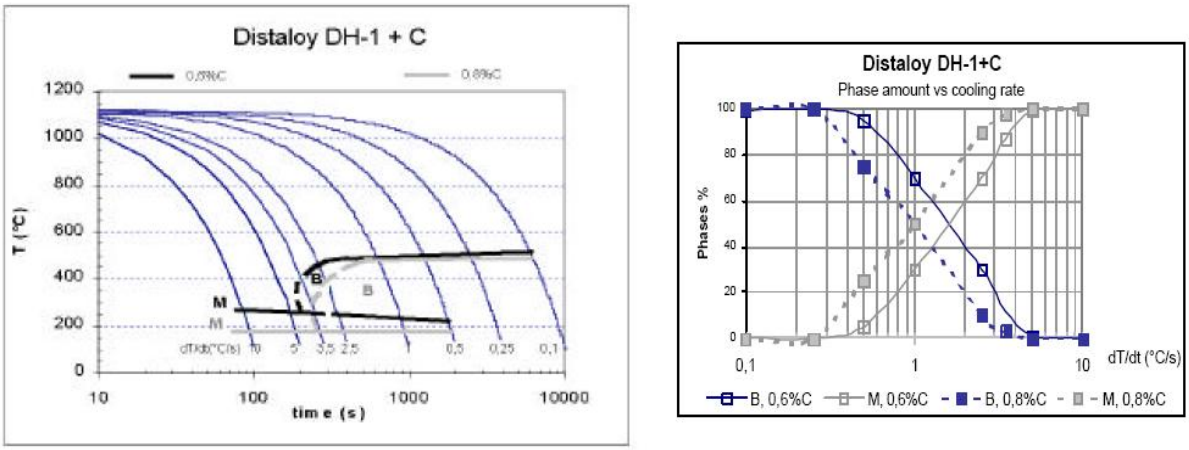

Figure 3 CCT and phase evolution Vs cooling rate curves for Distaloy DH with 0.6, 0.8%C [11]

Material	Density	Cooling rate, Hz	Bainite	Martensite
Distaloy DC	7.0-7.1	10	75	25
	7.0-7.1	60	1	99
	7.2-7.3	10	75	25
	7.2-7.3	60	1	99
Distaloy DH	7.0-7.1	10	40	60
	7.0-7.1	60	0	100
	7.2-7.3	10	35	65
	7.2-7.3	60	0	100

Table 1 Effect of cooling rate on amount of Martensite and bainite (adapted from [29])

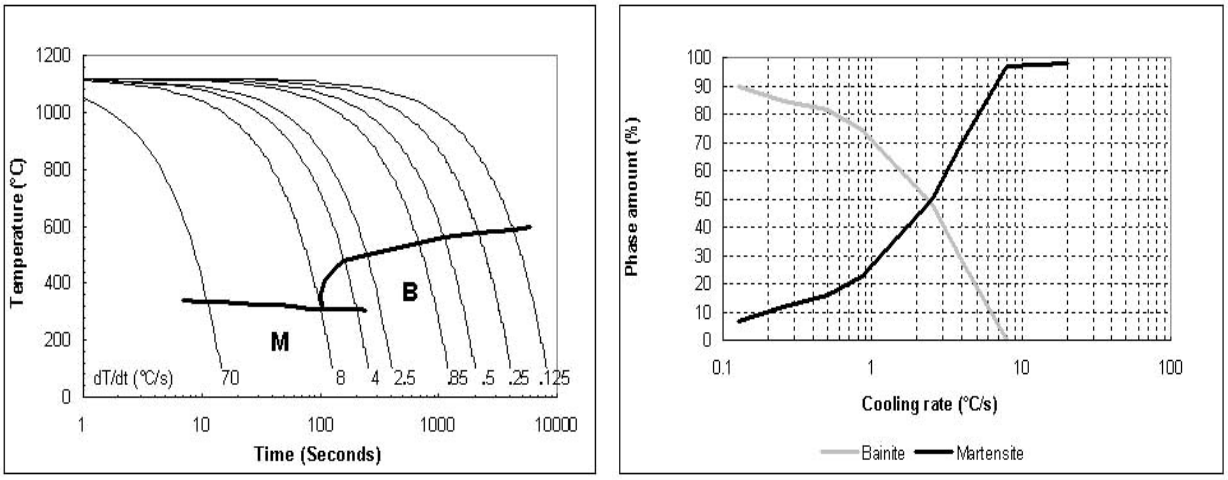

Figure 4 CCT and phase evolution Vs cooling rate curves for Distaloy DC with 0.5%C [29]

In another work, the authors reported that for Distaloy DH with 0.6 %C with a cooling rate of 7K/s the microstructure was majorly martensitic. The martensitic structure had a different morphology along with

traces of transforming austenite, upper bainite and very fine pearlite. Bainite and pearlite resolvable only by SEM and a hardness of 700 and 435 Vickers ($HV_{0.1}$) was reported for martensite and fine pearlite respectively. [26]

The above investigations have not considered the effect of sintering temperature and time on the resultant microstructure and mechanical properties. However, the effects of process parameters are dependent on the material and the alloying system. It is expected that that longer sintering times increase the hardenability, and hence can have an impact on strength but it can also increase the risk of surface decarburization. [30]

2.8 Residual Stresses

Residual stresses arise in materials due to non-uniform plastic deformation. Heat treatment processes can create non uniform plastic deformation which may be caused by temperature gradient or phase changes or a combination of both the factors. Residual stresses are a very serious problem in heat treatment, since they often result in distortion or cracking and in some cases in premature failure of the part in service. Considering the temperature gradient across the component during quenching, it is known that the surface is cooled more rapidly than the core, which results in a temperature gradient across the cross section. Since the surface will be at a much lower temperature than the core, it should undergo contraction more than the core. But the core prevents the contraction as much as it should and will therefore put the surface under tension while being in compression. When the part reaches ambient temperature the surface will have residual compressive stresses and the core will have residual tensile stresses.

The phase transformations during heat treatment are well understood and they play a major role in the development of residual stresses owing to the difference in density between parent and resultant phases, contributing to transformation plasticity. The austenite to martensite expansion accounts for the largest volumetric expansion, the lower the M_s temperature the greater the expansion [14]. It can be understood that while cooling from austenitizing temperature, normal contraction takes place until the M_s is reached, and between M_s and M_f the transformation of austenite to martensite causes volumetric expansion.

To understand the combined effect of temperature and phase changes for a through-hardening treatment, three stages during cooling can be considered. During the first stage the surface is prevented from contraction by the center and will be in tension while the center is in compression. During the second stage, the surface reaches M_s temperature and transforms to martensite with a volumetric expansion, while the centre is undergoing normal contraction due to cooling. Consequently, the core of the material will prevent the surface from expansion. During the final stage when the centre reaches the M_s, it expands and exerts tensile stresses to the surface. The residual stress at ambient temperature is stated to be larger when the austenite finishes transformation at a higher temperature; this is because thermal contraction strains can no longer be compensated by transformation plasticity once the austenite has decomposed [31].

Surface compressive residual stresses can improve the fatigue performance of the parts. Sinter hardening can be used to generate compressive residual surface stresses if proper process control is ensured. Controlling the distribution of carbon is necessary to obtain the desired stress state after sinter hardening. Higher cooling rate at the surface than at the core will usually result in a mixed microstructure of bainite and martensite s in the core. Subsequent martensite formation at the surface will induce compressive stresses. However, if the part is decarburized during sinter hardening process the carbon content at the surface will be lower than that at the core, which results in tensile residual stresses at the surface. Depletion of 0.1 wt. %C corresponds to ~50 ^{o}C increase in M_s temperature and hence carbon control is critical during sinter hardening as it governs the resultant surface stress state of the component.

2.9 Tempering

Tempering treatment improves the mechanical properties of sinter hardened steels and causes dimensional changes which will impact the final part size [3,24].The tempering process can be said to have three stages-

(I) Stress relieving associated with carbon diffusion. This occurs at relatively lower temperatures and at appreciable rates between room temperature and 200°C

(II) Transformation of retained austenite to bainite which is measurable at 100°C and extends to 300°C.

(III) Carbon diffusion out of martensite associated with formation of carbides above 200 ^{o}C [24].

The first and third phenomenon involves reduction in dimensions while the second phase results in volume expansion. For the case of wrought steels with 1%C the total shrinkage in length considering the first and third stages is in the order of 0.25%.

2.9.1 Phase Changes Associated with Tempering and their Effect on Physical Properties

The first stage of tempering is associated with carbide formation in the martensitic structure which is differentiated from that of the cementite phase. This is a phase which nucleates and grows more rapidly at low temperatures and in the highly strained condition. It has a *cph (i.e., hexagonal close packed)* crystal structure and nucleates preferably at subgrain boundaries inside martensite. These phases are extremely small in size, since they are formed at low temperatures and thus they can only be identified with the aid of electron microscope. The precipitation of epsilon carbides contribute to slight increase in hardness values. The increase being proportional to the carbon content which determines the quantity of the carbides, but the depletion of carbon from martensite contributes to softening. [24]

The second stage of tempering is associated with the transformation of retained austenite to bainite (between 100° to 300°C) consisting of ferrite and epsilon carbide. This is associated with a large, positive dimensional change and the amount of reaction varies linearly with the magnitude of length change. This bainite is different from decomposed martensite even though both constituents contain epsilon carbide. At this stage of tempering, the matrix is ferritic. The third stage is characterized by carbon diffusion from the martensite and also from the dissolution of epsilon carbides resulting in loss of tetragonality in martensite and formation of ferrite. Ferrite and cementite structure is formed at relatively short times

and low temperatures (of the order of 250°C [24]).The cementite is first formed as films at the boundaries of martensite plates and as globules and platelets inside the martensite plates. Later, the cementite tends to become spheroidal by diffusion at higher temperatures and increasing lengths of time. While the dissolution of epsilon carbides and removal of carbon from martensite soften the material the precipitation of cementite contributes to hardening. The softening of the specimen occurs when the reactions associated with the third stage of tempering become more prominent. A marked drop is observed at about 200°C in the case of wrought steels.

The alloying elements may enter the ferrite or carbides in varying amounts depending on the type and concentration of the elements. Some elements are not found in carbides-Cu and Ni included in this category; while Mn, Cr and Mo form carbides with a tendency in the order mentioned [24]. The alloying elements in steels tend to increase the resistance of steel to softening. This tendency is more significant in the case of carbide forming elements participating in the secondary hardening phenomenon [24].

3. EXPERIMENTAL METHODS

3.1 Materials

The experimental work was undertaken on different alloy steels from Höganäs AB to elucidate the effect of alloying on their Sinter hardening response. Table 2 displays the chemical composition of the investigated materials All the investigated samples were subjected to sinter hardening treatment. Compaction pressure for the powder was adjusted in order to achieve a final sintered density of 7.1g/cc. They were sintered at 1120°C for 30mins in $90N_2/10H_2$+0.2% CH_4 atmosphere. All samples were cooled at an average cooling rate of 2.5°C/s in the temperature range of 850 to 300°C, as shown in Figure 5.

Alloy composition	**Sample code**	**Carbon content (Wt. %)**
Astaloy Mo *Water-atomized Steel powder prealloyed with **1.5%Mo***	Mo	0.55
Distaloy DC *Astaloy Mo diffusion bonded with **2%Ni***	DC lower carbon content	0.55
Distaloy DC	DC higher carbon content	0.7
Distaloy DH *Astaloy Mo diffusion bonded with **2% Cu***	DH lower carbon content	0.55
Distaloy DH	DH higher carbon content	0.7

Table 2 Materials chemical composition

Figure 5 Average cooling rate measured for samples between temperatures 850-300°C- 25% fan speed

Afterwards, the sintered specimens were tempered at 200°C for 1 hour in air. All samples were admixed with 0.6 wt. % of lubricant (Kenolube). The cooling rate was controlled by setting a fan at the end of the furnace and the average cooling rate was determined by including a reference sample of known hardenability in the furnace and hence judging from the microstructures obtained in the reference sample, the average cooling rate was determined (2.5 °C/s).

3.2 Apparent Hardness Testing

Hardness testing was performed in accordance with *ISO 6507-1*. *Wolpert Dia Testor* hardness tester was used to perform the tests. The hardness class to which the test specimen belongs to was determined by Vickers hardness testing with a force of 49.03N corresponding to HV5. Vickers hardness number was calculated by dividing the applied load in kilograms force by the projected area of indentation in square millimeters. The area is computed from the mean of the measured diagonals of the indentations.

The materials were classified to be of the hardness class which has to be tested for HV10 values. Five acceptable indentations were made and the corresponding hardness values were calculated. The lowest hardness value was discarded while calculating the average. Indentations without clearly defined corners were not considered for measurement.

3.3 Tensile Testing

Tensile testing experiments were carried out in accordance with the *MPIF standard 10*. *Instron* Universal testing machine 4505R with Blue Hill-Instron software was used to perform the tests. An extensometer of 12.5mm length was used. The specimens tested were in as received condition and not machined. Flat bars were used for testing. The geometry of the tensile specimens is illustrated in Figure 6. Elongation to fracture was measure by the extensometer and care was taken so that the extensometer remained on the specimen until fracture. In addition, the 0.2% proof stress was determined. The tensile results were collected from five specimens that broke within the gauge length section. The strain rate was chosen as $0.0001s^{-1}$ in accordance with SS-EN 10002-1 (2001 standard). The standard suggests a strain rate equal to $10^{-4}s^{-1}$ for materials with a Young's modulus less than 150 GPa. The Young's modulus of all the investigated materials was less than 150 GPa.

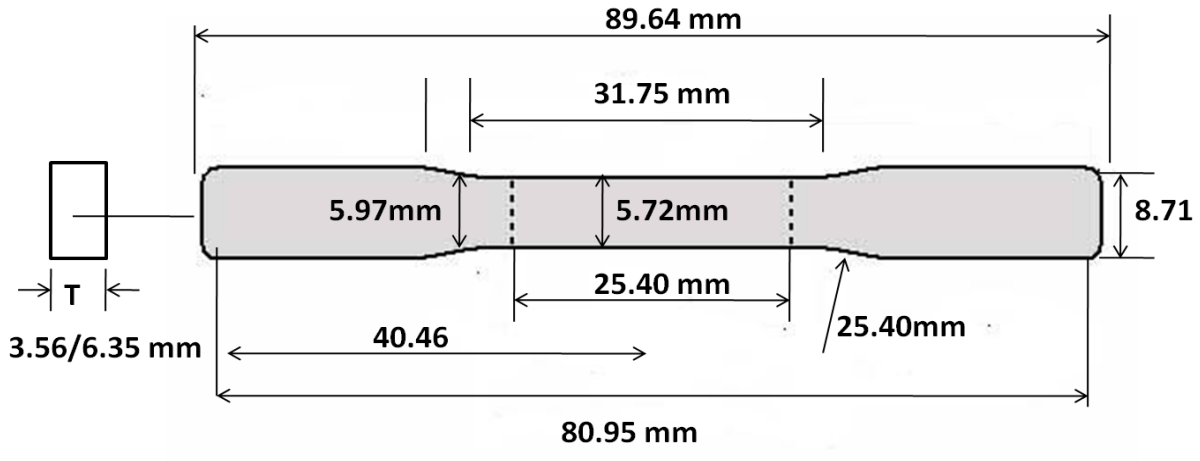

Figure 6 Flat test bar

3.4 Metallographic Examination

Samples for metallographic examination were cut from fractured tensile bars after tensile examination. All samples were embedded in *Polyfast* mounting resin from *Struers*. They were subjected to grinding down with 220µm grinding paper and a subsequent polishing with 9, 3 and 1µm diamond paste (is this according to Struers recommendation? If yes you can add that if you want). Distaloy DC and Distaloy DH samples were etched with nital (3 volume% HNO_3 in ethanol)while Astaloy Mo was etched with 10ml HCl and 3ml HNO_3 Microstructural gradient if any observed from etching is important to be determined as it can reflect varying carbon concentration and hence a residual stress state at the surface. The optical microscopy imaging and the image analysis of the samples was performed on *Leitz (Leica) DMRX* light microscope with mechanical stage and *Axiocam MRCS*.

3.4.1 Phase Amounts Analysis

Phase amounts were determined using *Axio Vision Image analyzer* (Carl Zeiss imaging solutions). All images considered for analyses were taken at 200X magnification. Ten representative images for each sample were analyzed. However, it is worthy to note that in any image analysis some percentage of error is inevitable, since the method is restricted to the resolutions limits of optical microscopy.

For Distaloy DC materials white areas which are a result of segregation of Ni were termed nickel rich areas (Ni-rich). Within different regions of the sample, the different phases were marked. The area (μm^2) of all the phases was summed using the *Areas sum* function. The total analyzed area of the individual phases was then divided by the defined measurement frame area. Consequently the volume fraction of individual phases was obtained in percentage.

3.4.2Porosity Analysis

The porosity analysis was carried out using *Axio Vision Image analyzer* (Carl Zeiss imaging solutions). All images considered for analyses were taken at 200X magnification.

Pore Area and Pore Shape Factor (PSF)

For these measurements, samples were only finely polished and at least 1500 pores were analyzed from each sample. Pore area was calculated by the *area sum* function mentioned in the phase amounts calculation. Pores were marked, and for each pore the area was obtained in μm^2. The pore area distribution for each measurement was obtained.

In general shape factors are tools to quantify a deviation of the analyzed object from the ideal or a modal one. Circularity is chosen as a good solution to quantify the objects in metallographic images exhibiting complex shapes. Hence, the shape factor of pores i.e., the roundness has been calculated according to equation 4

$$PSF = 4\pi S/P^2 \qquad \text{Eq. 4}$$

Where *P* is the perimeter and S is the area of each pore. This formula has been used previously for the same purpose for instance in [26,32]. The range of PSF is $0<PSF\leq1$. PSF equal to 1 indicates a perfectly round shape and the closer is the value to 1, the more irregular is the pore shape. The shape factor is very sensitive to any irregularity of circular objects but it is almost completely insensitive to small

elongation [33]. Pores less than 10µm length of contour were disregarded from evaluation due to the limitations in digital imagining abilities making their evaluation unreliable.

3.5Microhardness Testing

Microhardness testing is generally used for evaluation of the hardness specific phases, microstructural constituents and regions or gradients too small for apparent hardness testing. In this method an indentor is forced into the specimen under carefully controlled conditions and under prescribed loading. It is followed by measuring the depth of penetration and assigning a hardness number. This number is calculated as indenting force divided by the projected area of the resulting indentation. The softer the material the greater will be the penetration of the indentor.

In a porous material, the measurements are performed in the pore free areas, indicative of the hardness of the material while avoiding the influence of porosity. The hardness instrument used was a *Schimadzu HMV-2000* microhardness tester equipped with a Vickers diamond pyramid (included angle of 136°) indentor and a provision for measuring the length of the indentation of diagonals with a precision of 0.1 micrometer

The load to be chosen depends upon the range of hardness expected in the materials as well as the desired accuracy levels. Large indentations reflect smaller errors in analysis; however, too large indents may include different phases, even pores resulting in flawed measurement. After indentation trails for selecting the optimum load, a load equal to 0.1 Kgf was selected. To confirm the nature of observed phases, microhardness measurements have been made on etched surfaces. Hardness profiles were also measured from the outer surface to the core to detect any possible carbon gradient. In steels, different microstructures have different hardness values, see Figure 7.

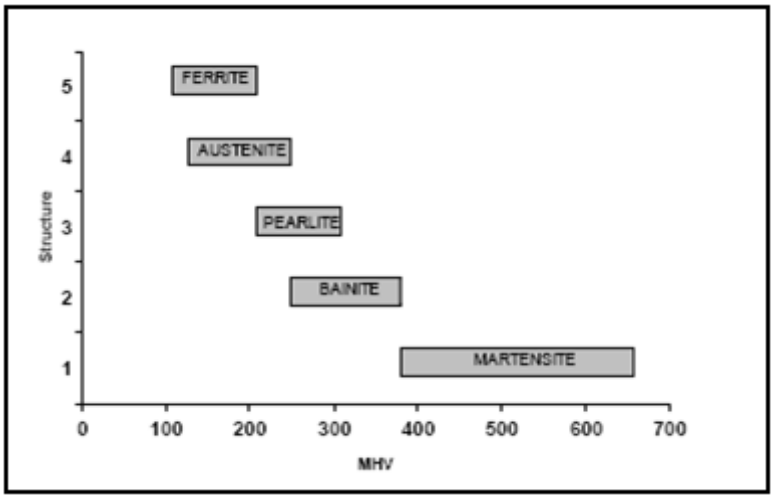

Figure 7 Microhardness range for different microstructures in steel [7]

In order to detect hardness gradient in the investigated samples, microhardness indentations were made from the outer edge of the specimen towards the centre. Since there could be possibilities of carburization/decarburization during sintering, the indentations were taken from the surface which was

exposed to the sintering atmosphere towards the center of the sample. Corresponding to each distance in the microhardness profiles, five measurements were taken. The average value was plotted and the standard deviation values were also indicated.

3.6Residual Stress Measurement

X-Ray Diffraction (XRD) technique was used to perform residual stress measurements. X-ray technique for stress measurements is based on linear-elastic method; wherein, change in lattice spacing *d* (this distance between crystallographic planes is used as a strain gage) is measured. This distance (i.e. d) is basically used as a strain gage from which the residual stress can be calculated measured. Hence, the residual stress determined by XRD is the arithmetic average stress over the volume of the material defined by the irradiated beam. The interplanar spacing can be calculated using the Bragg's law given in equation 5.Thus, knowing the X-ray wavelength λ and the angle of reflection θ (θ is measured experimentally) the *d*-spacing is then calculated. The letter n in equation 5 is the order of reflection which can be any integer.

$$n\lambda = 2d\sin\theta \qquad \text{Eq. 5}$$

This method is confined to the surface (for subsurface measurement electropolishing is used to expose new surfaces) of the sample and a condition of plane stress is assumed to exist in the exposed surface layer. No stress is assumed perpendicular to the surface and the stress distribution is hence described by the principal stresses, $\sigma_1$and σ_2, existing in the plane of the surface. However, a strain component perpendicular to surface exists from the contraction caused by the two principle stresses from the Poisson's ratio. For plane-stress model, the unstressed lattice spacing (d_o) need not be known precisely and can be substituted with the *d*-spacing measured for the specimen at Ψ (psi) =0.

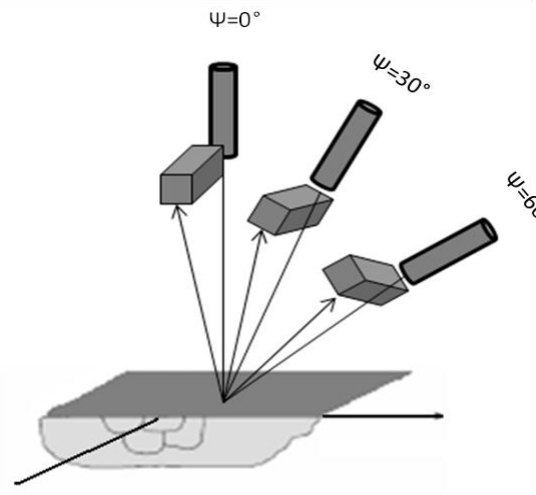

Figure 8 Residual Stress Measurement using XRD

The strain in the sample from the principle stresses (σ_1 and σ_2), defined by the angles φ and Ψ is computed from the *d*-spacing according to linear elasticity equations (assuming biaxial stresses):

$$\frac{d_{\varphi\psi} - d_o}{d_o} = \left[\left(\frac{1+\upsilon}{E}\right)_{hkl} \sigma_\varphi sin^2\psi\right] - \left[\left(\frac{\upsilon}{E}\right)_{hkl}(\sigma_1 + \sigma_2)\right] \quad \text{Eq.6} \tag{34}$$

where d_o is the stress-free lattice spacing and $d_{\varphi\psi}$ is the spacing between the lattice planes measured in the direction defined by φ and ψ. The strain is expressed in terms of the changes in linear dimensions of the crystal lattice (Left Hand Side). In equation 6, (1+υ/E) and (υ/E) correspond to the elastic constants for the crystallographic direction normal to the lattice planes in which the strain is measured by (*hkl*). The surface stress σ_ϕ can hence be calculated measuring $d_{\varphi\psi}$ from the fundamental linear relationship between lattice spacing and $\sin^2\psi$, given by the slope of the plot in equation 6. In the $\sin^2\psi$ technique, lattice spacing is therefore determined for multiple ψ tilts and a straight line is fitted. The linearity is attained by least squares regression method and the slope of the best fit line is calculated as the residual stress value. [34,35]

In this work, the residual stress analyzer used was XSTRESS 3000 manufactured by Stresstech The machine produces X-rays with known wavelength λ and provides a penetration of about 20µm. A beam diameter of 3 mm was used for the measurements. Measurements were carried out at varying angles of Ψ (Figure 8). The residual stress values along a given direction are computed by the XSTRESS 3000 software and *d* (which is $d_{\varphi\psi}$) versus $\sin^2\psi$ is plotted automatically, the slope of which is either positive or negative indicating tensile or compressive stresses respectively. Precision in measurement depends on many factors including the positioning of the sample which has to be aligned with the beam and the appropriate calibration of the instrument. The X-ray source in this investigation was Cr Kα with a wavelength of 2.290920 Å. The residual stress was measured by calculating the lattice strain of ferrite {211} planes. In this study, the ψ angle was varied between -45° and +45°.

3.7 Scanning Electron Microscopy

Scanning electron microscopy (SEM) was performed using high resolution field emission SEM, LEO 1550 Gemini equipped with secondary electron, backscattered electron, in-lens and energy dispersive X-ray (EDX) analysis detectors. Compared to optical microscopy, much better resolution and depth of focus, and much higher magnifications can be attained using SEM. Qualitative and quantitative chemical analyses were performed using EDX and a Link INCA system. To compliment the EDX point analysis, X-ray elemental mapping was performed.

High magnification images of individual phases in the microstructure were obtained. By means of EDX, point analyses, line scan and elemental mapping the distribution of Ni and Cu was investigated Representative regions of the microstructure were chosen to perform EDX analysis and within each region different phases of microstructure were analyzed. The composition (normalized) obtained from these analyses were tabulated.

4. RESULTS

4.1 Microstructure

4.1.1 Light Optical Microscopy

4.1.1.1 Astaloy Mo

From the optical microscopy investigation of etched Astaloy Mo sample, Figure 9 (a), (b) , it was observed that it had a bainitic microstructure. Throughout the sample, the microstructure was homogeneous, typical of prealloyed materials. No evidence of microstructural gradient between surface and centre of the specimen was seen. The microstructure of all the samples analyzed also show pores (indicated by P in the figure), but a detailed study on porosity is presented in section 4.5.

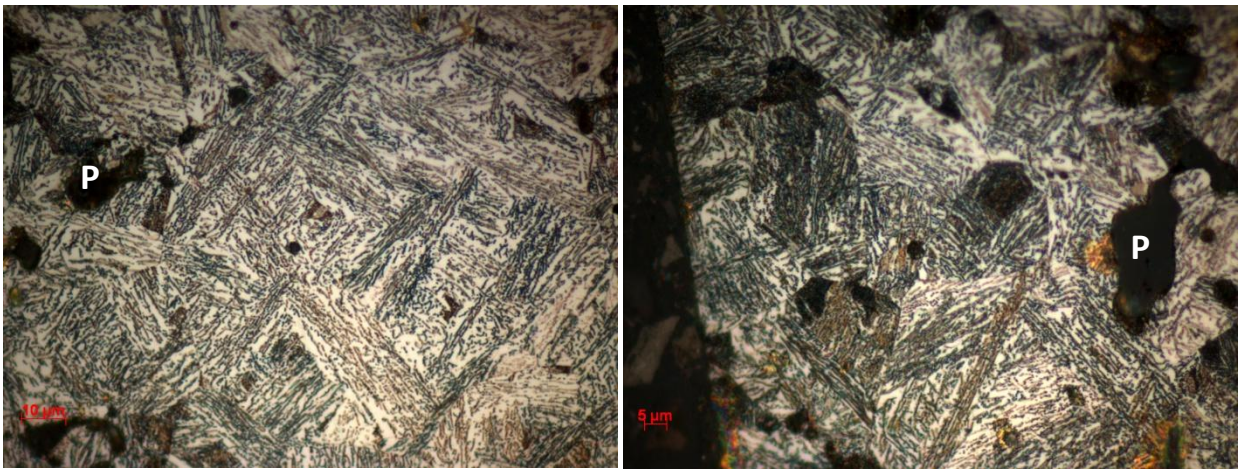

Figure 9(a) Astaloy Mo- Bainitic Microstructure (Centre) (b) Astaloy Mo- Surface Microstructure, Bainite

4.1.1.2Distaloy DC

Microstructural investigation of Distaloy DC, Figure 10(a), (b) & Figure 11(a), (b), suggests a microstructure, with regions of martensite (indicated by M in the figure)-etched light brown, bainite (indicated by B in the figure)-etched blue and nickel-rich areas etched white. Similar regions were identified at both carbon levels. An increase in the amount of martensite was observed with an increase in carbon content from 0.55% to 0.7%. Comparison of the amounts of phases is presented in the *phase amounts analysis* section 4.1.2.

4.1.1.3Distaloy DH

This material was etched with a Nital solution. The results for microstructural analysis of Distaloy DH are presented in Figure 12 & Figure 13. Distaloy DH showed bainitic-martensitic microstructure at both carbon levels. The amount of each phase is estimated using image analysis as mentioned earlier is presented in section 4.1.2.

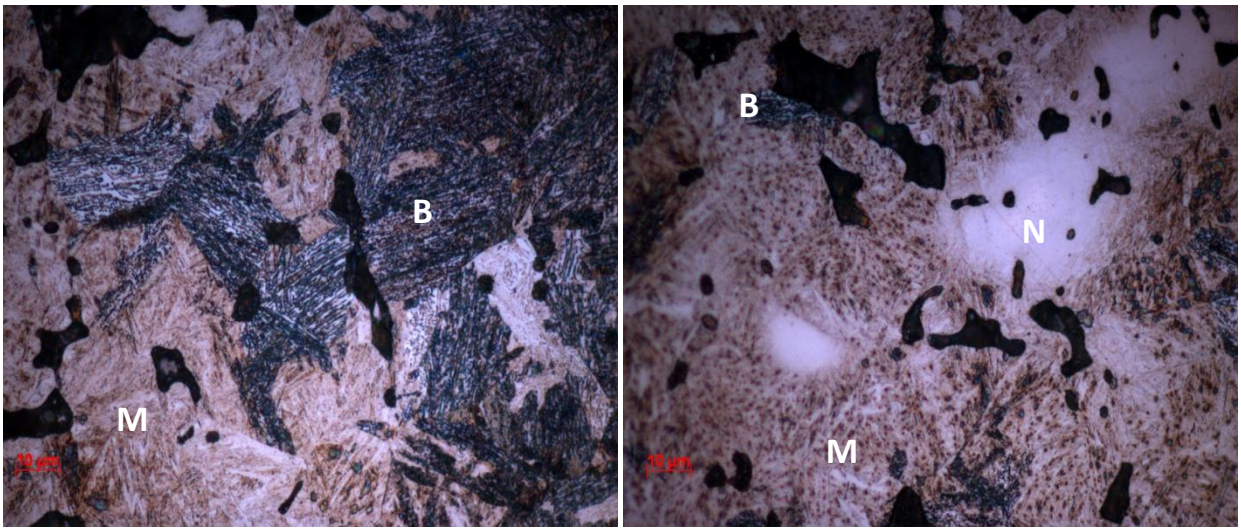

Figure 10(a) Distaloy DC+0.55%C- Bainitic (B)-Martensitic (M) regions (b) Distaloy DC+0.55%C Nickel Rich (N) areas

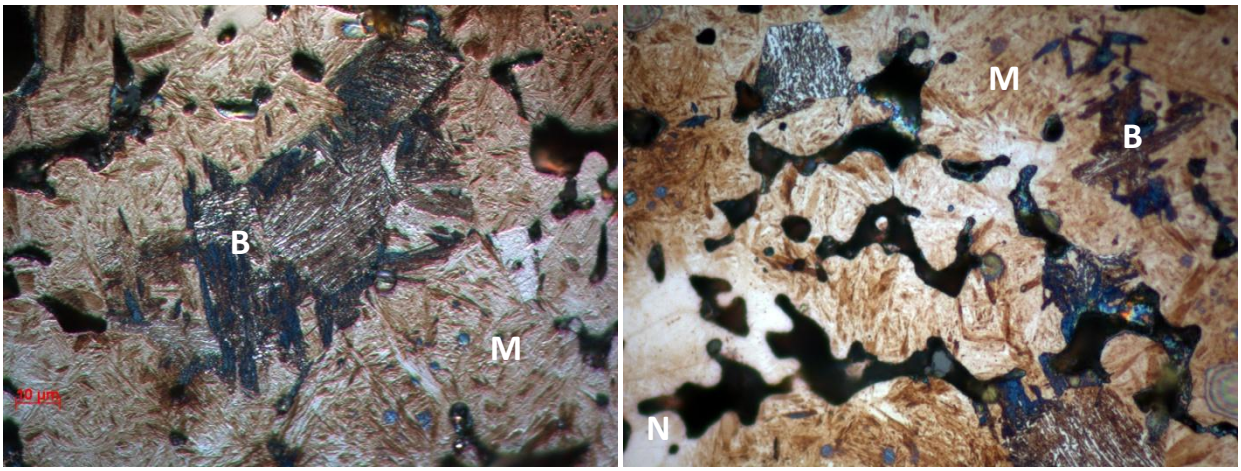

Figure 11 (a) Distaloy DC+0.7%C Bainitic (B)-Martensitic (M) regions (b) Distaloy DC+0.7%C Ni-Rich (N) areas in the Microstructure

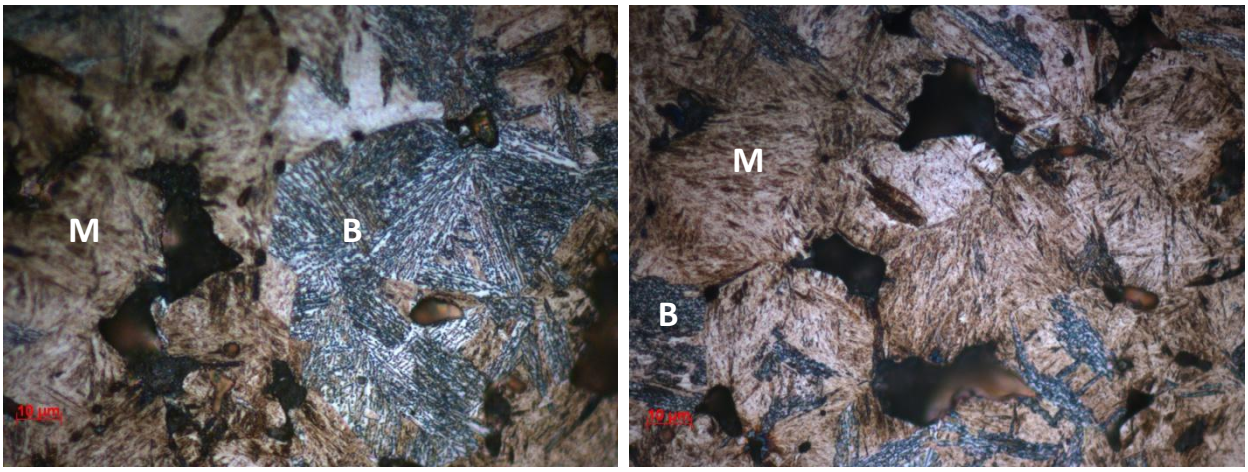

Figure 12(a) Distaloy DH+0.55%C Bainitic (B) Martensitic (M) regions (b) Distaloy DH+0.55%C Microstructural features

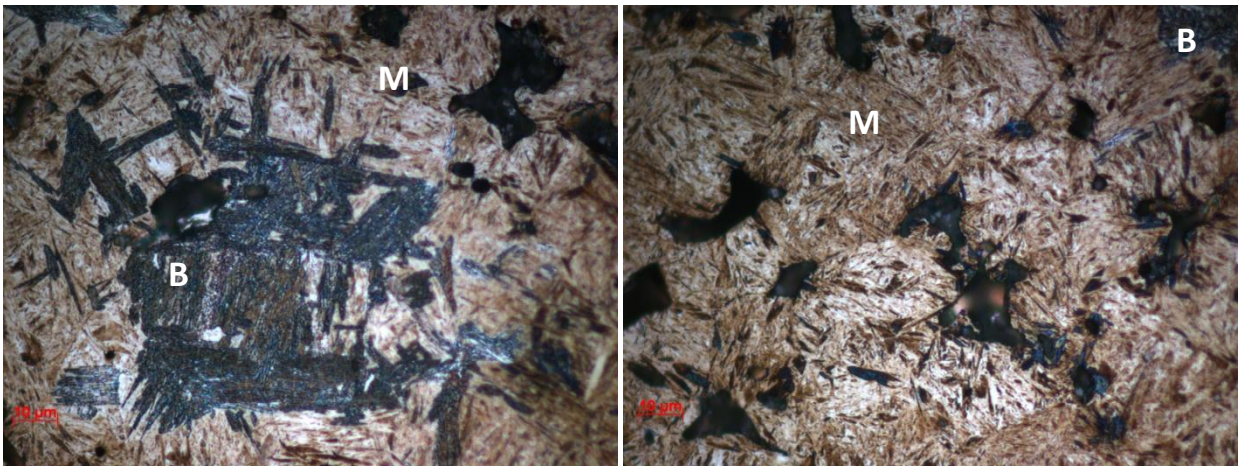

Figure 13(a) Distaloy DH+0.7%C Bainitic-Martensitic Microstructure (b) Distaloy DH+0.7%C Microstructure

4.1.2 Phase Amounts Analysis

From the phase amounts analysis it was observed that Astaloy Mo had almost a completely bainitic microstructure. In Distaloy DC specimens, nickel rich areas were detected. For Distaloy DC the amount of martensite increased from 59 vol. % to 80 vol. % with an increase in carbon content from 0.5 wt. % to 0.7 wt.%. The volume percentage of bainite decreased from 36 vol. % to 16 vol. % with the increase in carbon content.

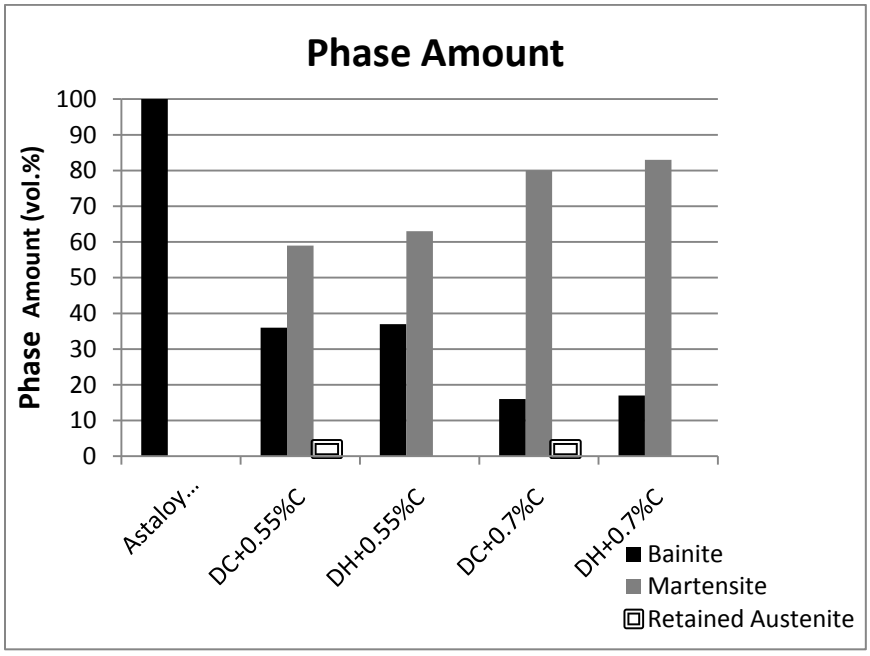

Figure 14 Phase Amounts Measurement results from Image analysis

The Ni-rich area volume seems to be the similar at both carbon levels. On the other hand, with the same carbon increase and concentrations as for Distaloy DC; Distaloy DH martensite content increased from

63vol.% to 83 vol.% and bainite decreased from 37 vol.% to 17 vol. %, Distaloy DH,. Thus, the results indicated that at both carbon levels, Distaloy DH had higher martensite content and lower bainite content than that of Distaloy DC.

4.2 Tensile Testing

The results from tensile testing are summarized in Figure 15. Ultimate tensile strength, 0.2% proof stress and elongation results for the investigated alloys are discussed in this section under separate sub-headings. For the results presented in figure 15, error bars correspond to the standard error of mean.

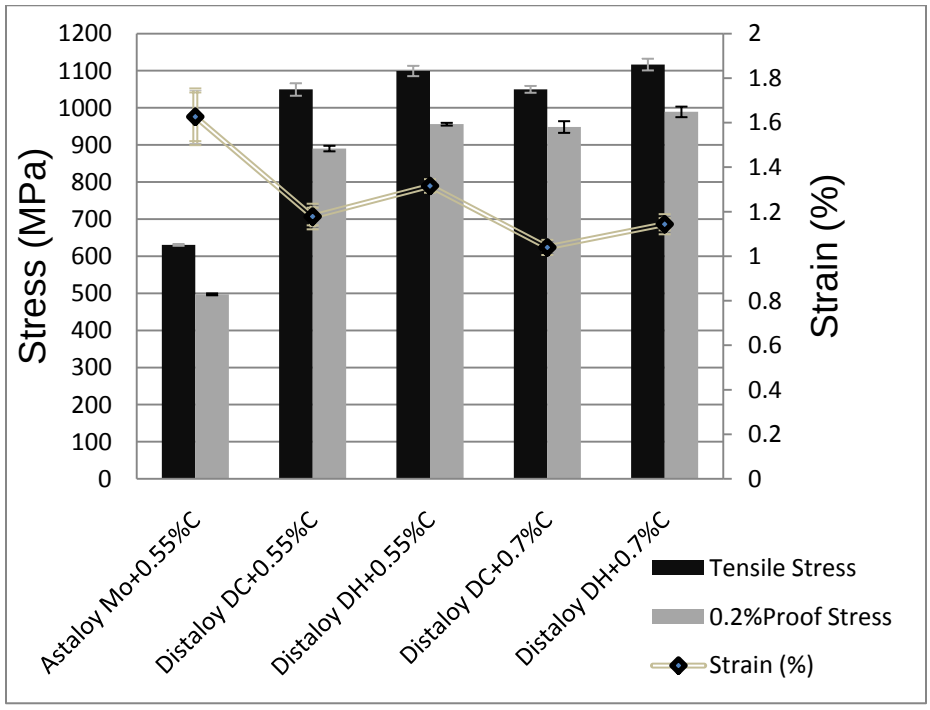

Figure 15 Mechanical Properties of Investigated alloys

4.2.1 Ultimate Tensile Strength (UTS)

The ultimate tensile strength (UTS) values were calculated from the tensile test results, which is the maximum stress value in the Engineering stress versus strain curve. From the results (Figure 15) obtained, Astaloy Mo had the lowest value, 630 MPa. Distaloy DC alloys exhibited similar values for UTS at both higher and lower carbon levels, i.e.an average value of 1050 MPa. Distaloy DH alloys showed a slightly higher average UTS value than that of Distaloy DC (at both carbon levels). The average values obtained for Distaloy DH alloys were ~1100 MPa.

4.2.2 Elongation

Astaloy Mo was found to have the highest elongation to fracture (~1.6%). With an increase in carbon content the elongation decreased for Distaloy DC from ~1.2 at 0.5 wt. %to ~1% at 0.7 wt. % carbon. This decrease was observed for Distaloy DH samples as well, see Figure 15.

4.2.3 0.2% Proof Stress

The proof stress values were calculated graphically from the stress strain curves and the results are plotted in Figure 15. It was seen that Astaloy Mo possesses the least value among the alloys with 497 MPa. For Distaloy DC with an increase in carbon content the proof stress increased from 890MPa to 948MPa; and for Distaloy DH a corresponding increase from 956 MPa to 989 MPa is observed.

4.3 Apparent Hardness

The results of the apparent hardness testing are illustrated in Figure 16. It can be seen that Astaloy Mo had the lowest hardness. At lower carbon level (i.e. 0.55 wt. %), Distaloy DC exhibited a slightly higher hardness than Distaloy DH. The case was reversed at higher carbon content. The apparent hardness increased with increase in carbon content for both Distaloy grades. However, the increase was more significant for Distaloy DH. The error bars correspond to the standard deviation values.

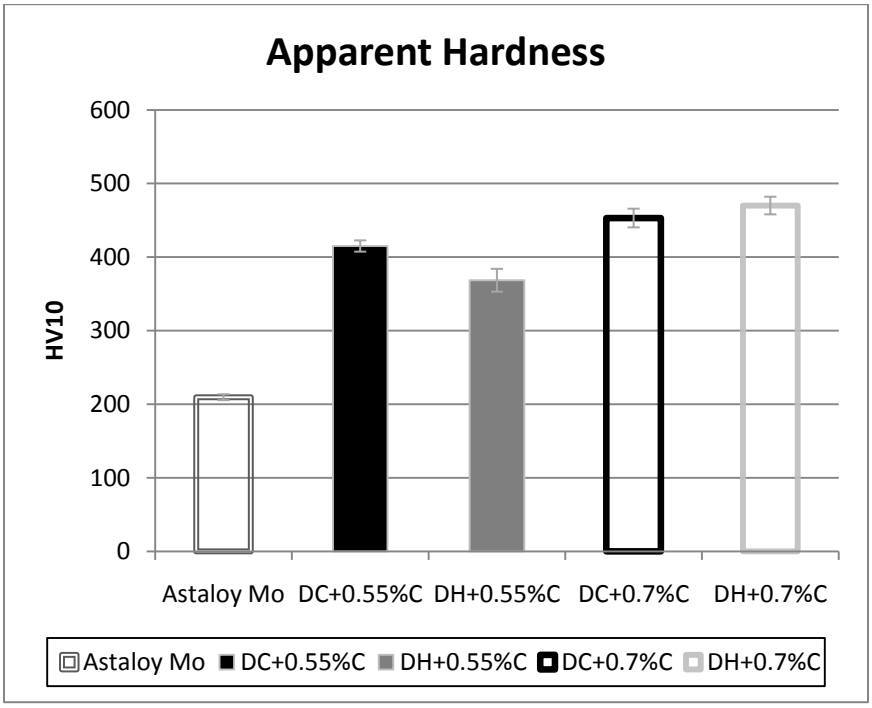

Figure 16 Apparent Hardness Measurements

4.4 Microhardness Testing

The microhardness results are shown in Figure 17. The error bars correspond to standard deviation of mean. All microhardness values correspond to $HV_{0.1}$. It can be seen that Astaloy Mo with a fully bainitic structure had a microhardness value 300 Vickers (For Distaloy DC alloys, with the increase in carbon content the hardness of the bainite phase is increased from 287 (at 0.55 wt.%C) to 356 Vickers (at 0.7 wt.%C). However, the increase in hardness for the martensitic phase was not significant; frpm650 (at 0.55 wt. %) to 676 (at 0.7 wt. %) Vickers, see Figure 17. The hardness values for the Ni-rich areas (which were etched white) was found to be 200 and was measured to be the same at both carbon levels. For Distaloy DH, the increase in average microhardness values ($HV_{0.1}$) for bainite and martensite was from

246 to 284 and 476 to 724 respectively. . At the lower carbon level, the martensite phase had a lower hardness in Distaloy DH than that in Distaloy DC; whereas, at 0.7 wt. %C the martensite phase in Distaloy DC showed slightly higher hardness than that in Distaloy DH. The bainite phase has almost a similar hardness in all three steel grades.

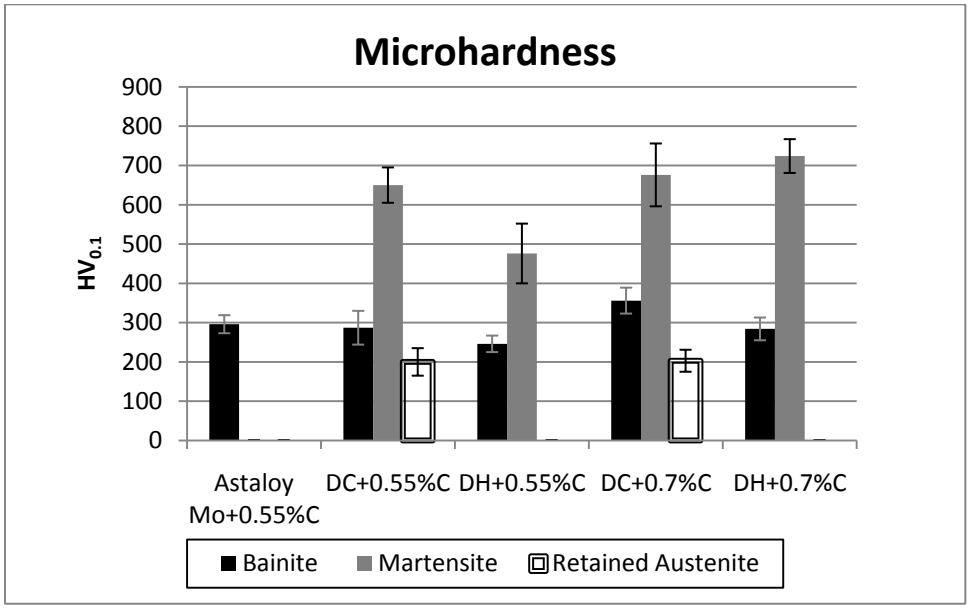

Figure 17 Microhardness measurement results on individual phases of the microstructure

4.4.2. Microhardness Profiles

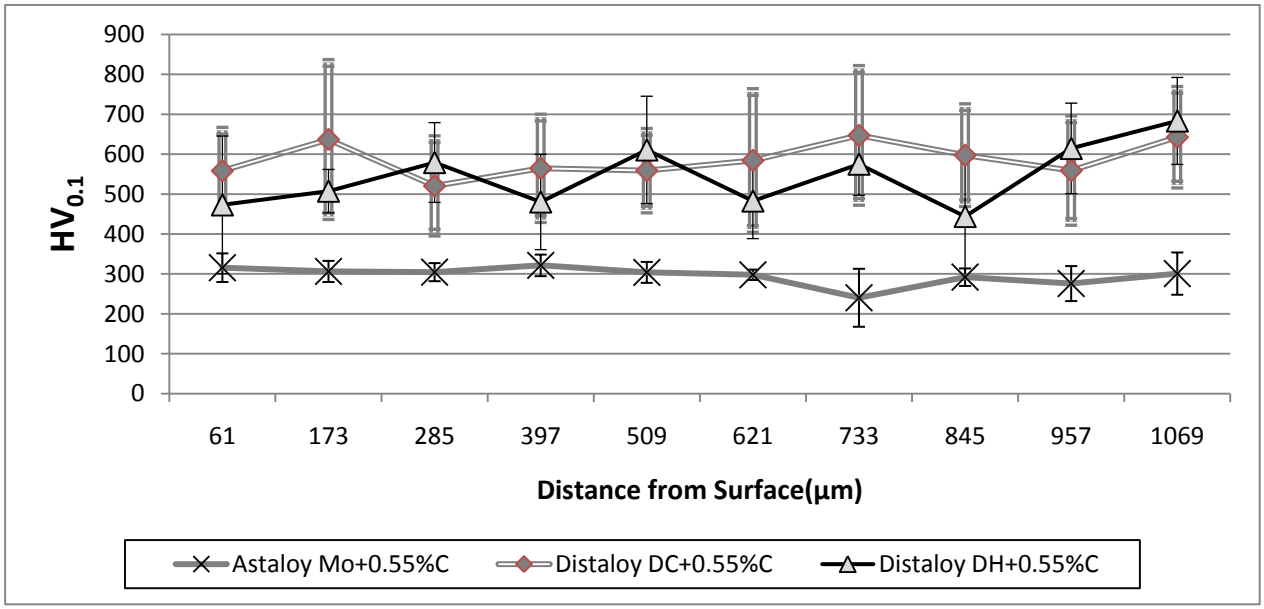

Figure 18 Microhardness Profile measurements from the surface of the specimen towards the centre

No specific pattern was observed from the hardness profiles. The results indicated a heterogeneous microstructure for Distaloy grades, whereas, for Astaloy Mo the scatter in the hardness values was much less, hence, suggesting a homogenous microstructure. The error bars in Figure 18 refer to standard deviation values. No indications of surface carburizing or decarburizing could be observed. For Astaloy Mo within 60µm of the surface more measurements were made using 5 and 10gms load and the indents did not show any hardness gradient within this distance from the surface.

4.5 Porosity Analysis

4.5.1. Pore Area Analysis

The pore area analysis results are presented in Figure 19. The results for the pore area range of 1-10 μm^2 are not reliable as they are below the resolution limits of the optical microscope and hence, they will not be discussed. However, from figure 19 it can be seen that Astaloy Mo had majority of its pores, nearly 85% volume fraction, within 10 and 1000μm^2. In addition, between 10-1000 μm^2, both Distaloy DC and Distaloy DH showed higher volume fraction of pores with 0.7 wt. % of carbon than with 0.55 wt. % of carbon. All materials had a very low fraction of pores greater than 1000 μm^2

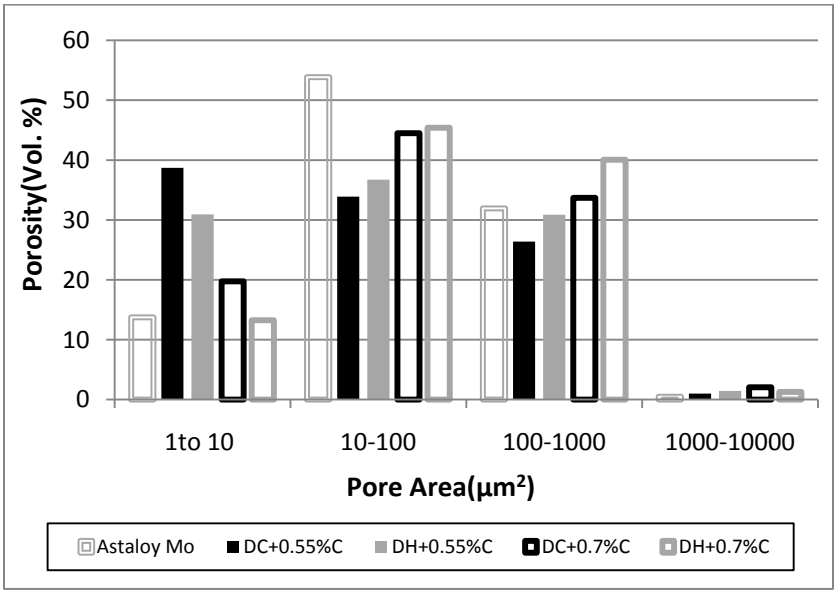

Figure 19 Results from Pore Area analysis for the investigated alloys

4.5.2 Pore Shape Analysis

From pore shape analysis, Figure 20, the volume fraction of round pores corresponding to PSF=1 was observed to be higher for Distaloy DC than Distaloy DH. In addition, Figure 20 shows that as the PSF deviates from 1, alloys with 0.7 wt. % of carbon have a higher volume fraction of pores as compared to alloys with 0.55 wt. % of carbon.

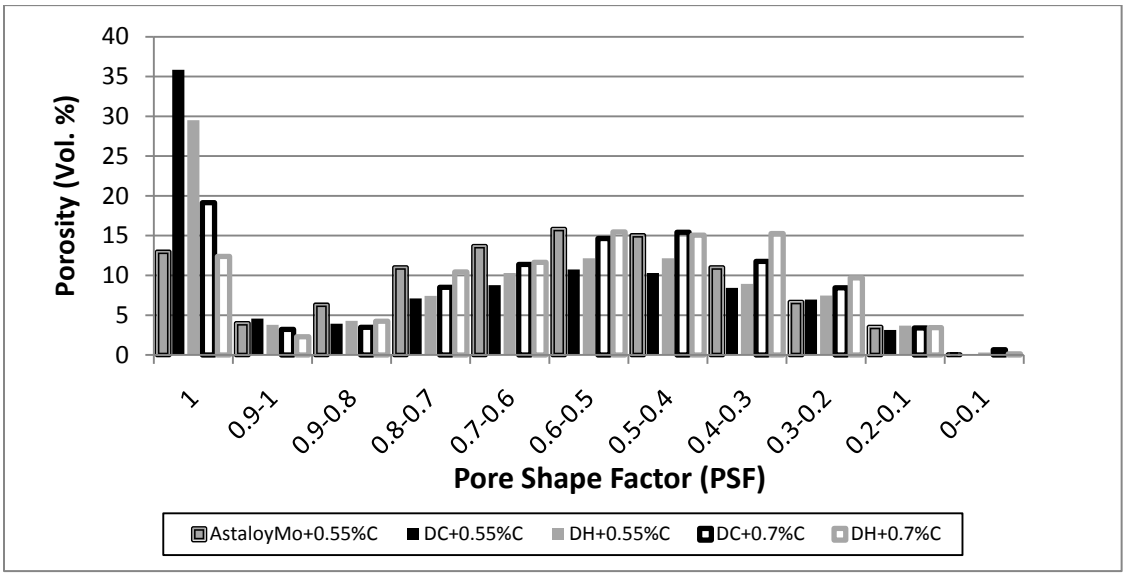

Figure 20 Pore Shape Factor calculations from Image Analysis

4.5.3 Pore Shape Factor versus Pore Area

Mean PSF was plotted against pore area for different ranges of pore size. The results obtained are shown in Figure 21. It was observed that the values corresponding to the highest mean PSF (PSF =1) were for pores lying within an area range of up to 10µm^2 (smallest size of pores). As mentioned previously, this range of pore size is below the resolution limits of optical microscopy and thus the values plotted for this range should not be fully trusted. However, from Figure 21 it can be seen that the larger pores are more irregular and vice versa. In addition, as illustrated in Figure 21, all materials seem to have similar pore rounding behavior during the investigated sintering treatment.

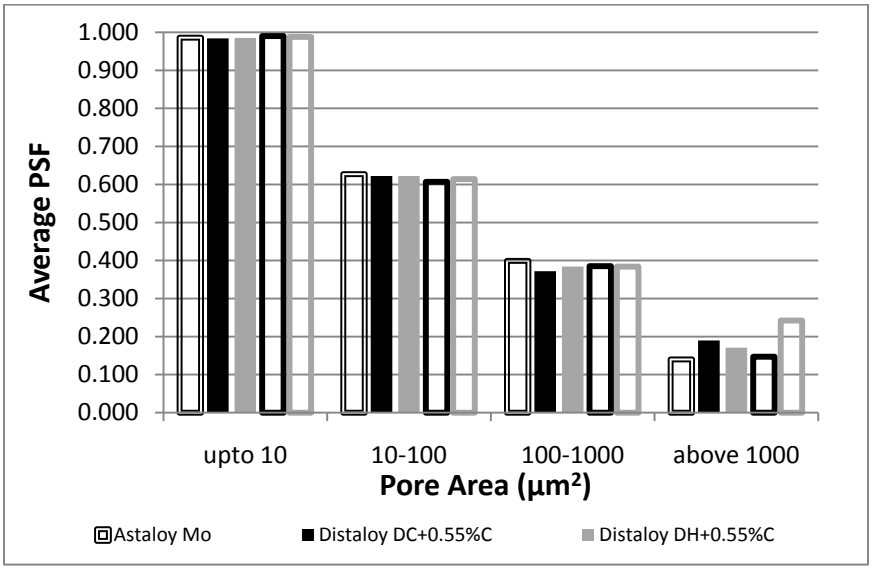

Figure 21 Mean PSF versus Pore Area

4.6 Residual Stress Measurement

The results from the residual stress measurement indicated that Astaloy Mo possessed compressive surface residual stresses. The other materials had tensile residual stresses. However, the tensile stress values exhibited by these samples were not profound in magnitude. Also, no specific trend was observed with respect to the amount of carbon and these stresses.

Material	Residual Stress (MPa)
Astaloy Mo+0.55%C	-47.8±4.1
Distaloy DC+0.55%C	12.8±6.3
Distaloy DH+0.55%C	27.0±2.5
Distaloy DC+0.7%C	32.3±3.4
Distaloy DH+0.7%C	38.5±7.0

Table 3 Results from the Surface Residual Stress Measurements

4.7 Scanning Electron Microscopy (SEM)

4.7.1.1Astaloy Mo

Homogenous microstructure was observed for Astaloy Mo. The sample exhibited a fully bainitic microstructure as discussed in the *section 4.1* even around the pores. Figure 22 depicts the structure of the alloy. In the images pores as well as grain boundaries can be distinguished. The image to the right is a high magnification image of the central portion in Figure 22.

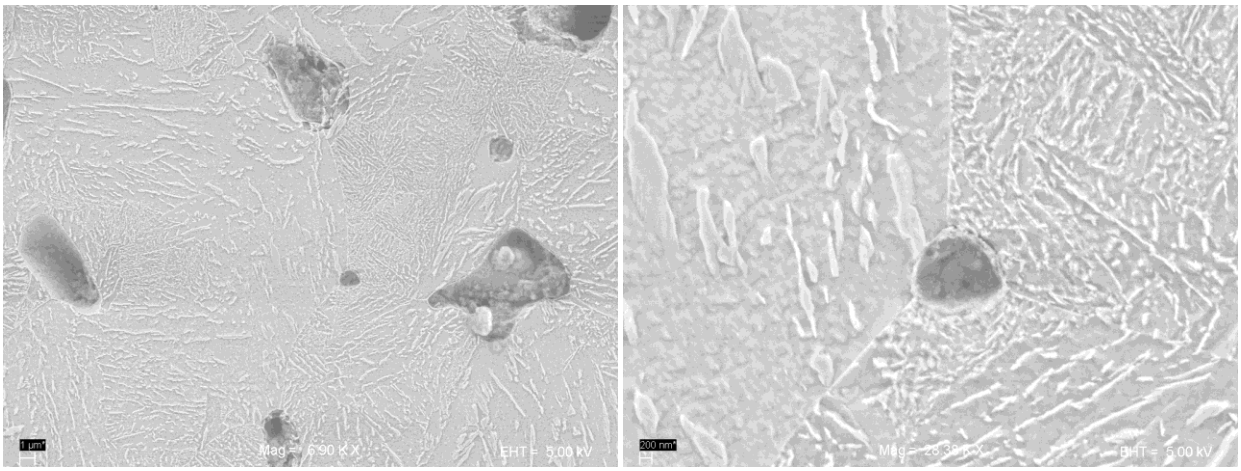

Figure 22 Bainitic microstructure in Astaloy Mo. Left: Low magnification, Right: High magnification

4.7.1.2 Distaloy DC

The microstructure for Distaloy DC materials consisted of bainite, martensite and Ni-rich areas as mentioned in section (give the number of section. The nickel rich regions remain unetched as shown in Figure 23. In addition, these regions were analyzed using EDX line scans, and as illustrated in Figure 25, a higher concentration of Ni in these regions is clear. The bainitic and martensitic micro-constituents in Distaloy DC are shown in Figure 24 . These phases were similar for both the lower and higher carbon levels of the alloy, however the amount of each phase varied.

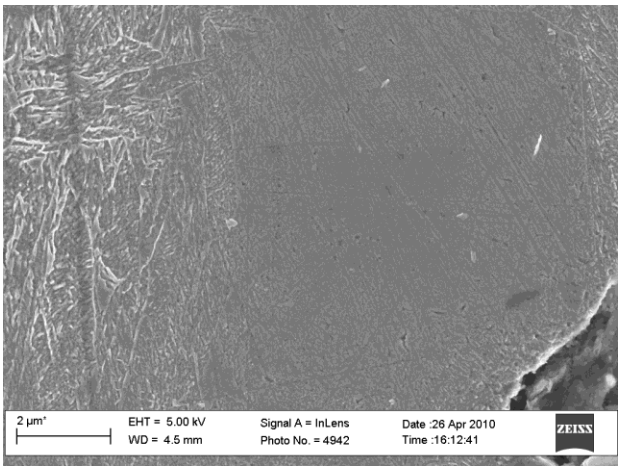

Figure 23 Ni-Rich Region in Distaloy DC Materials remain un-etched

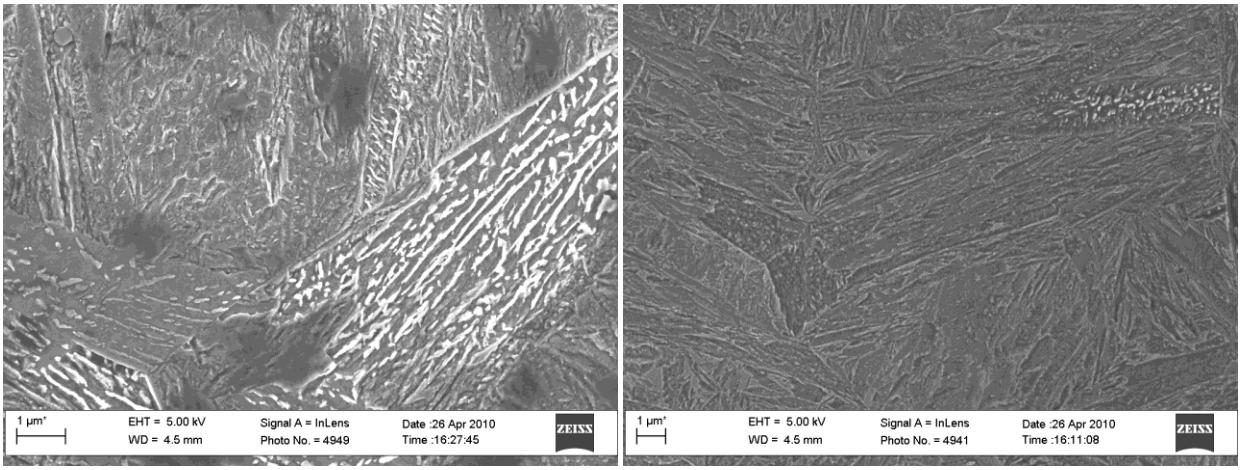

Figure 24 SEM images of Microstructural features in Distaloy DC: Left-Bainite (white features-carbides) Right- Martensite

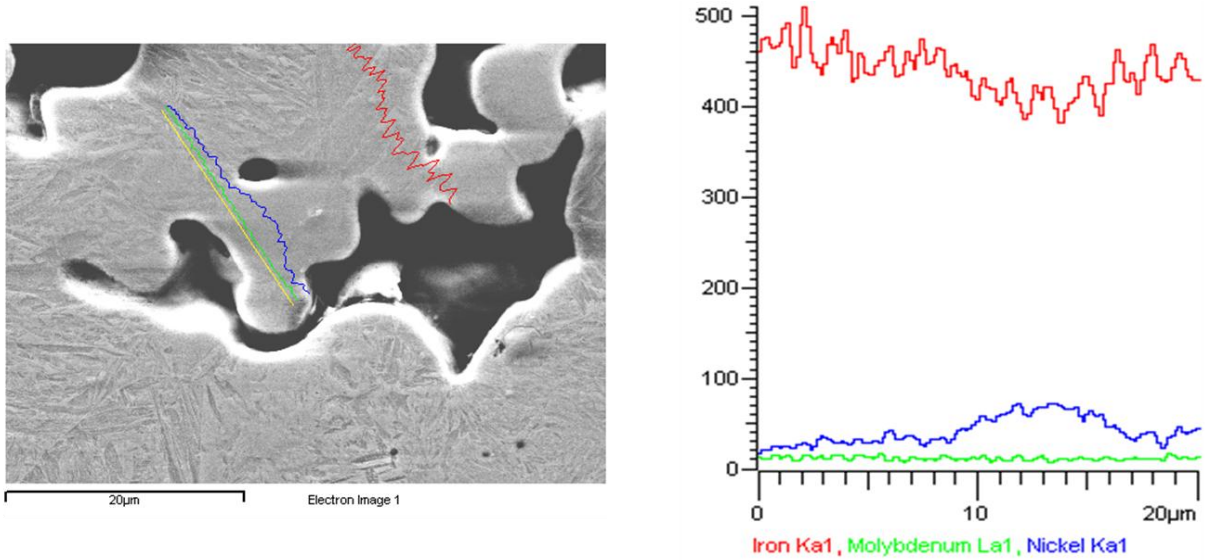

Figure 25 EDX line scan performed on an un-etched feature in Distaloy DC corresponding to Ni-rich region

Distaloy DH

Distaloy DH materials as mentioned earlier had bainitic and martensitic microstructure and these are shown in the SEM images illustrated in Figure 25 and Figure 27. These structures were similar for DH+0.55%C and DH+0.7%C and only the amount of phases varied by increasing the carbon content.

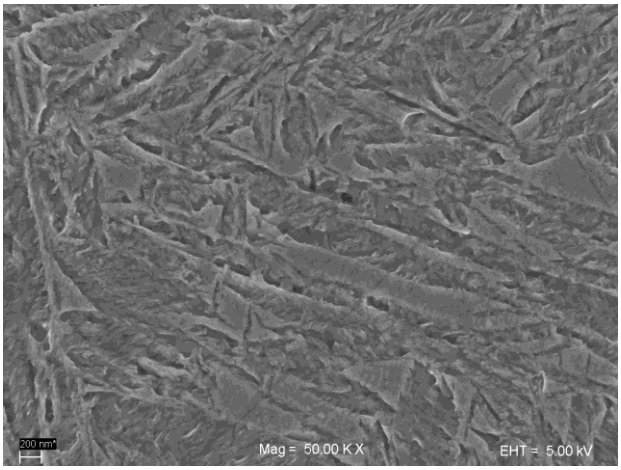

Figure 26 Martensitic microstructure in Distaloy DH

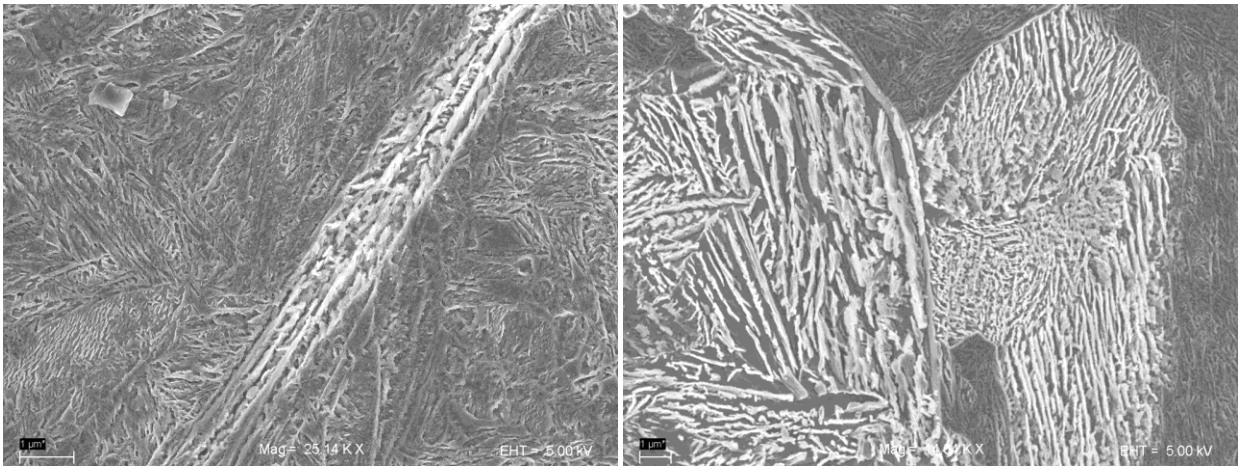

Figure 27 Bainitic Microstructure in Distaloy DH materials

EDX Analysis Results

In order to understand the effect of addition of Cu and Ni as well as their distribution, EDX analyses (i.e. point analysis and elemental mapping) were performed. The results are illustrated in Figure 28-31.The carbon content was not analyzed in the EDX analyses as this technique is not sensitive enough to light elements such as carbon. All chemical compositions obtained from the EDX analyses were normalized to 100 percent. The following figures are examples of the results of the analysis obtained. Each figure has an image of region, with numbers corresponding to the points where EDX point analysis was performed. The respective results are tabulated at the right corner after EDX analysis. An image from the same region was analyzed for elemental maps and is placed adjacent to the first figure. The corresponding elemental maps of this region are then presented. The maps obtained and the tabulated values are in agreement with each other.

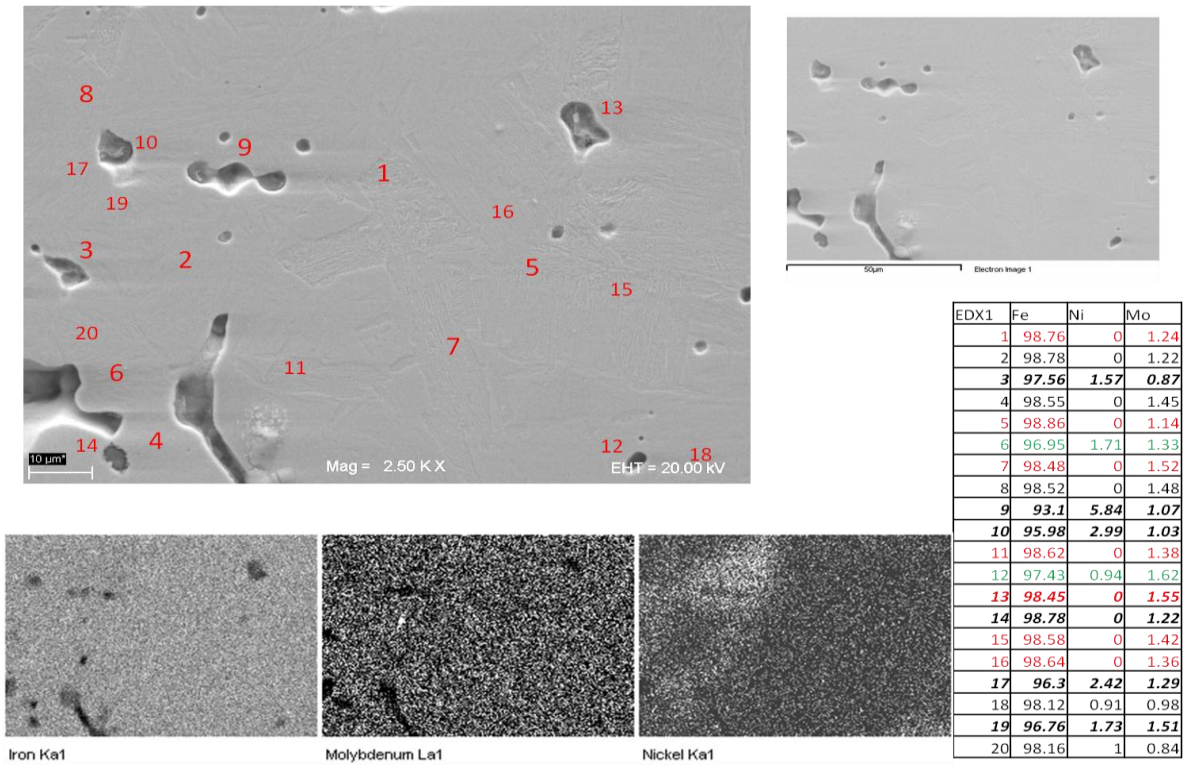

EDX1	Fe	Ni	Mo
1	98.76	0	1.24
2	98.78	0	1.22
3	***97.56***	***1.57***	***0.87***
4	98.55	0	1.45
5	98.86	0	1.14
6	96.95	1.71	1.33
7	98.48	0	1.52
8	98.52	0	1.48
9	***93.1***	***5.84***	***1.07***
10	***95.98***	***2.99***	***1.03***
11	98.62	0	1.38
12	97.43	0.94	1.62
13	***98.45***	***0***	***1.55***
14	***98.78***	***0***	***1.22***
15	98.58	0	1.42
16	98.64	0	1.36
17	***96.3***	***2.42***	***1.29***
18	98.12	0.91	0.98
19	***96.76***	***1.73***	***1.51***
20	98.16	1	0.84

Figure 28 EDX analysis and corresponding elemental maps of a region in Distaloy DC+0.55%C

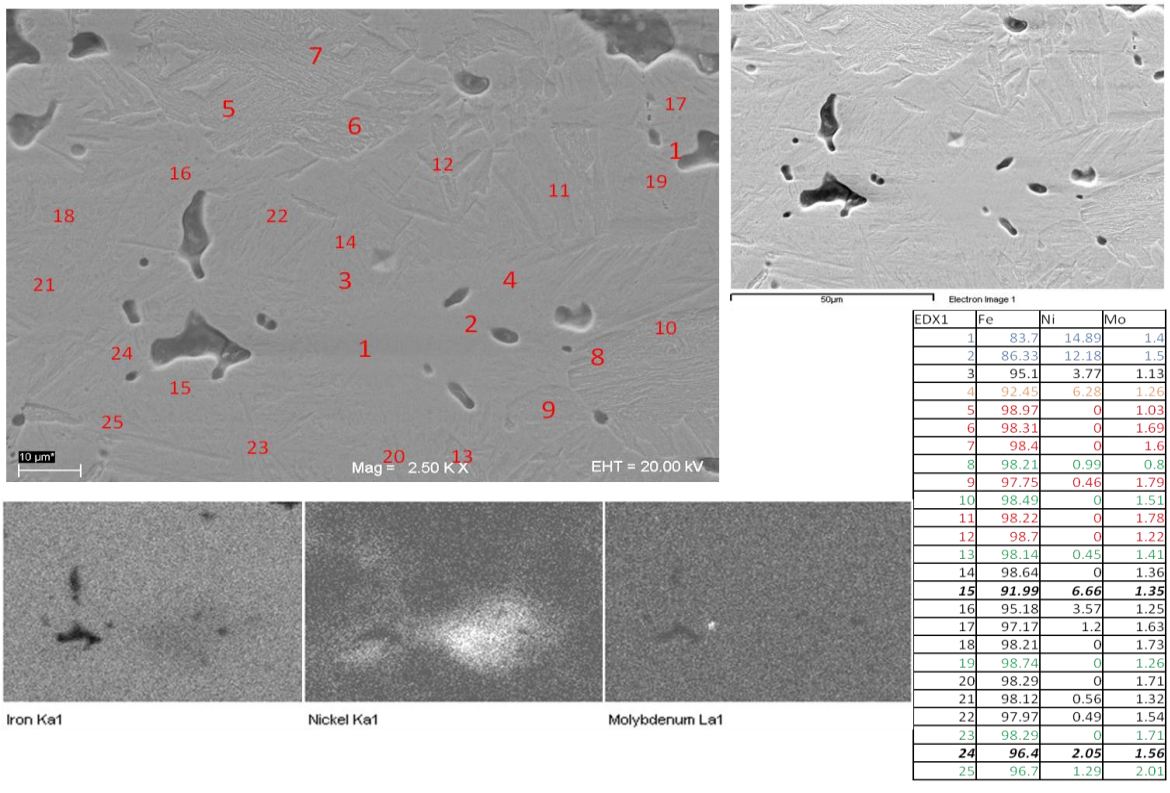

EDX1	Fe	Ni	Mo
1	83.7	14.89	1.4
2	86.33	12.18	1.5
3	95.1	3.77	1.13
4	92.45	6.28	1.26
5	98.97	0	1.03
6	98.31	0	1.69
7	98.4	0	1.6
8	98.21	0.99	0.8
9	97.75	0.46	1.79
10	98.49	0	1.51
11	98.22	0	1.78
12	98.7	0	1.22
13	98.14	0.45	1.41
14	98.64	0	1.36
15	***91.99***	***6.66***	***1.35***
16	95.18	3.57	1.25
17	97.17	1.2	1.63
18	98.21	0	1.73
19	98.74	0	1.26
20	98.29	0	1.71
21	98.12	0.56	1.32
22	97.97	0.49	1.54
23	98.29	0	1.71
24	***96.4***	***2.05***	***1.56***
25	96.7	1.29	2.01

Figure 29 EDX analysis and corresponding elemental maps of a region in Distaloy DC+0.7%C

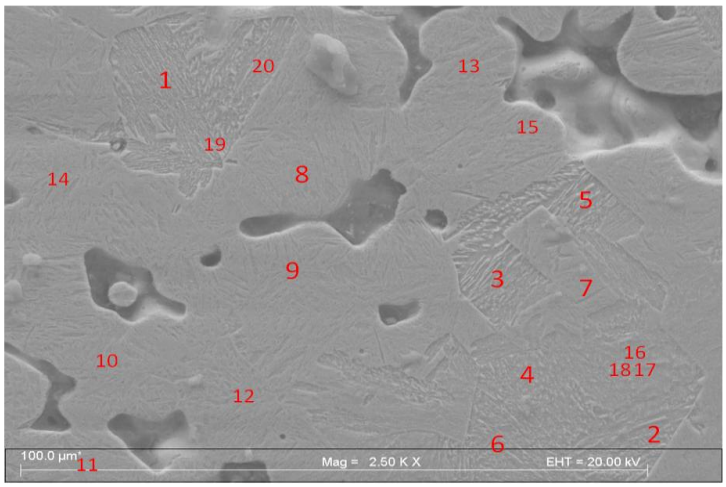

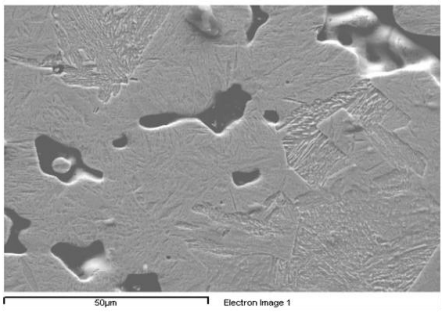

EDX3	Fe	Cu	Mo
1	98.48	0	1.52
2	98.68	0	1.32
3	97.67	0.73	1.6
4	98.45	0	1.55
5	***95.8***	***2.19***	***1.97***
6	98.71	0	1.29
7	98.77	0	1.23
8	95.8	2.72	1.48
9	95.85	2.35	1.79
10	93.62	4.41	1.96
11	95.77	2.76	1.47
12	96.73	1.75	1.52
13	96.17	2.57	1.26
14	95.71	2.87	1.42
15	***96.41***	***2.48***	***1.11***
16	-	-	-
17	98.58	0	1.42
18	-	-	-
19	98.29	0	1.71
20	97.71	0.6	1.68

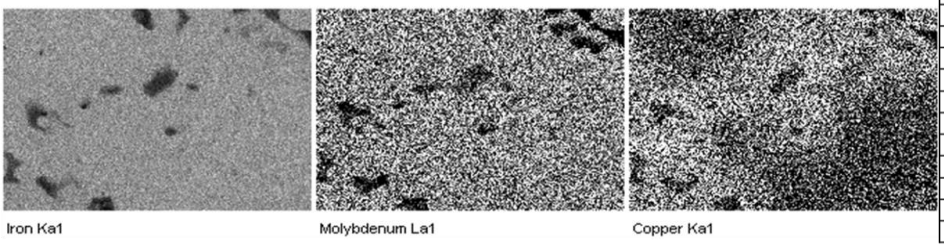

Figure 30 EDX analysis and corresponding elemental maps of a region in Distaloy DH+0.55%C

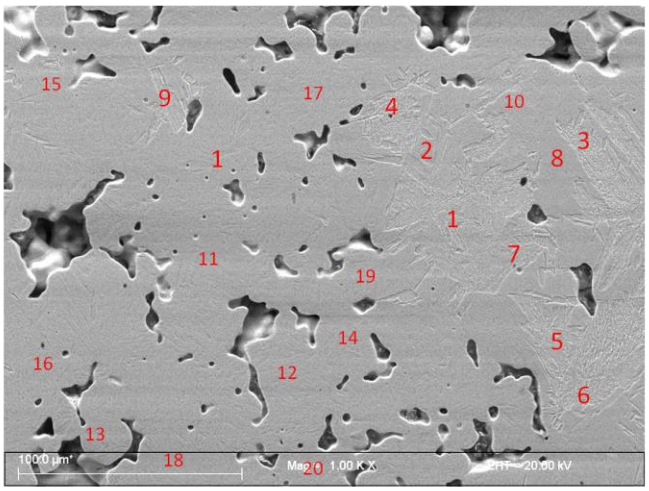

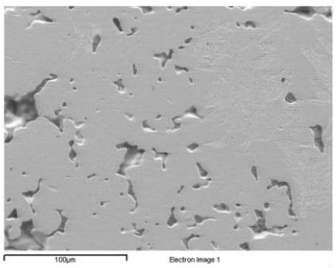

EDX2	Fe	Cu	Mo
1	99.02	0	0.98
2	98.32	0	1.68
3	98.55	0	1.45
4	98.26	0	1.74
5	98.24	0	1.76
6	-	-	-
7	99.01	0	0.99
8	98.56	0	1.44
9	98.83	0	1.17
10	98.98	0	1.02
11	98.01	0.91	1.08
12	97.26	1.56	1.18
13	***96.8***	***1.42***	***1.78***
14	94.06	4.26	1.68
15	96.94	1.69	1.37
16	93.63	4.13	2.24
17	95.78	3.23	0.99
18	98.24	0	1.76
19	96.9	1.53	1.57
20	95.35	3.42	1.23

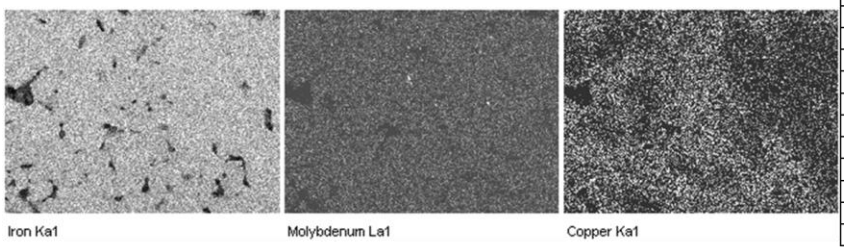

Figure 31 EDX analysis and corresponding elemental maps of a region in Distaloy DH+0.7%C

The following observations can be made from the results obtained using EDX point analyses and elemental mappings:

- Ni-rich regions were present in Distaloy DC, where as no Cu-rich regions were found in Distaloy DH.
- The bainitic microstructure in both Distaloy DC and Distaloy DH did not contain any of the diffusion bonded alloying elements, that is, Ni and Cu respectively. The absence of Cu and Ni within the bainitic regions of the microstructure was observed in both the alloys at both carbon levels.
- In Distaloy DC and Distaloy DH despite the fact that martensitic regions were mostly containing Ni and Cu, respectively, martensitic regions without any amount of Ni and Cu was also detected
- Pores were mainly surrounded by martensite; however, there were also bainitic regions present around the pores.
- There were regions with bainitic microstructure within a martensitic matrix and vice- versa with lesser or equal to the amount of Cu and Ni than that present in the martensitic regions.
- There were some regions within DH with 5-6 wt. %Cu but were difficult to resolve since they possessed martensitic microstructure not different from the other martensitic regions.

5. DISCUSSION

Microstructure

Astaloy Mo had a homogenous microstructure which was completely bainitic. Distaloy DC and Distaloy DH had a mixed microstructure with bainite and martensite at both carbon levels (0.55 wt. % and 0.7 wt. %) (Figure 9 to Figure 14). This implies that the cooling rate employed, 2.5°C/s, was not enough to obtain martensite in the microstructure for Astaloy Mo. Nor was the cooling rate enough to obtain a completely martensitic microstructure structure for Distaloy DC and Distaloy DH. An increase in hardenability through alloying or an increase in cooling rate would hence be necessary to achieve the same. These results are in agreement with previous findings, wherein according to the CCT curve it could be seen that with 0.6%C (which is more than what is used for the present case) a cooling rate close to 4°C/s was necessary to obtain martensite with Astaloy Mo [7]. Previous work on Distaloy DC and Distaloy DH reported that for the cooling rate used in this study, 0.8 wt. %C is necessary to obtain more than 90%martensite Distaloy DH [11]. In another work, for Distaloy DC with 0.7 wt. %C completely martensitic microstructure was achieved but at a cooling rate of 5-6°C [29].

The homogeneity in microstructure for Astaloy Mo is a consequence of the prealloyed nature of the powder, and is also evident from the microhardness profile for this material, shown in Figure 18. Apart from the presence of Ni-rich regions in Distaloy DC, the amount of bainitic and martensitic volume fractions measured for Distaloy DC and Distaloy DH were almost similar at both carbon levels An increase in martensite volume with an increase in carbon content was observed, and was similar for both the materials(Figure 14). This is because with respect to increasing hardenability carbon as an alloying element has the highest impact (equation 2) [5].

Distribution of Alloying Elements

Ni and Cu differ primarily in their response to sintering (mechanism of sintering). Copper melts at 1083°C i.e., below the sintering temperature, and the arising liquid phase is pulled by the capillary forces into the narrow gaps between particles of the solid component. The liquid copper also penetrates into the grain boundaries, since this leads to the minimization of the free energy of interfaces. Afterwards, Cu diffuses relatively easily into the iron powder particles [5,7,17]. Nickel however, has a melting temperature (1455 °C) well above that of the sintering temperature. Thus, solid state diffusion takes place for Ni which is slower than that of the liquid phase sintering for copper.

Microstructure for Distaloy DC consists of Ni-rich areas, seen from the metallographic investigation and the optical microscopy images (Figure 10,Figure 11,Figure 23 and Figure 25). In addition, the metallographic observations on the Ni-rich regions were then conformed by EDX analyses, see Figure 25. Presence of these areas within the microstructure is a result of the slow diffusion rate of Ni in Fe [5,7]. These features influence mechanical properties [21,26,36]. According to previous studies Ni-rich areas have been categorized into three different types: ferritic, martensitic and austenitic [36]. Ni-rich areas containing 11-23 wt. % Ni with hardness between HV170 and HV260 have been identified to be austenitic [21,36]; this is the case for the current study, since the hardness of the Ni-rich regions are around HV200, see Figure 17.

Regarding the distribution of alloying elements, it was observed that Mo was uniformly distributed within the microstructure for Distaloy DC and Distaloy DH at both the carbon level. In Distaloy DH and Distaloy DC in the bainitic regions of the microstructure, Cu and Ni (diffusion alloyed elements) were absent in the case of Distaloy DH and Distaloy DC respectively. This was observed for the alloys at both carbon levels (see Figure 28 to Figure 31). It is known that re-distribution of alloying elements does not occur during bainitic transformation as the transformation temperature is not high enough for the diffusion of these elements to occur [37]. These areas hence might have resulted due to the diffusion bonded nature of alloying, which imparts inhomogeneity in their distribution during sintering. Hence the regions without Cu and Ni possess lower hardenability and undergo bainitic transformation. On the other hand, in regions where the diffusion bonded elements are present and distributed, transform into martensite, due to their higher hardenability.

Since the total content of the diffusion bonded alloying elements for both Distaloy DC and Distaloy DH is similar (2wt %), average composition of Ni distributed within martensitic regions (excluding Ni-rich) is lower than that of Cu; since some of the Ni is arrested at the Ni-rich areas for Distaloy DC. As mentioned previously, Ni is less uniformly distributed in the microstructure when compared to Cu due to its lower diffusivity into iron. However assuming a homogeneous distribution of elements in wrought condition, the Jominy hardenability simulations using *JMatPro (5.0)* software shows a higher hardenability for a material with a chemical composition similar to Distaloy DC than a wrought material having the composition of Distaloy DH, see Figure 32.For this simulation the austenitization temperature was set to 950 °C and the austenite grain size was assumed to be 50 µm (Figure 32).

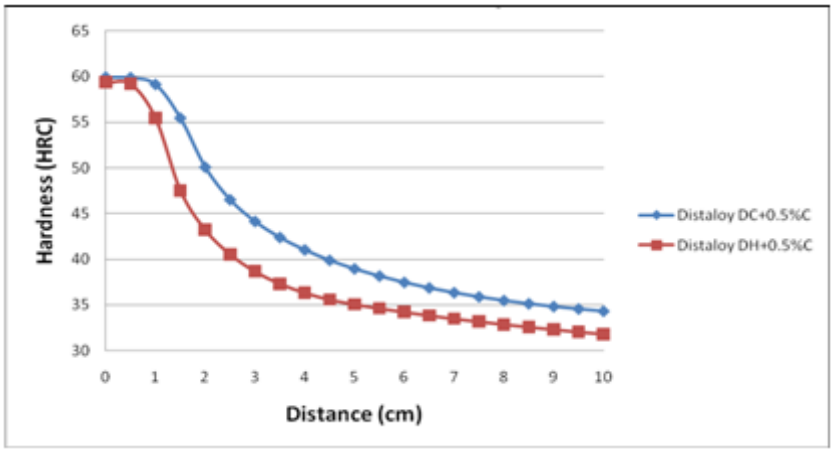

Figure 32 Simulated Jominy hardenability curves generated by JMatPro for wrought alloy composition equivalent to Distaloy DC and Distaloy DH

Ni increases the chemical activity of carbon; it induces a repelling effect and results in carbon diffusing away into neighboring regions around the Ni-rich areas [36].The direction of atomic migration is governed by the gradient of chemical potential, not by the concentration gradient as stated by the Fick's first law [38]. Atomic migration will occur from the region of high chemical potential to the region of low chemical potential. It is expected that regions around the nickel rich areas, even though leaner in nickel, can transform into martensite due to the improved hardenability contributed by the diffused carbon from this repelling effect. Higher hardness for martensite phase at the lower carbon content for Distaloy

DC could be due this effect. The martensite might have contained areas which have been hardened by excess carbon from the repelling effect, contributing to higher hardness. Also Ni deficient areas having martensitic structure around Ni-rich regions could be noticed from the SEM analysis results.

Ni and Cu deficient regions were present within the martensitic microstructure in these alloys at both carbon levels. Thus, these martensitic regions (lacking Cu and Ni) are supposed to be comparable to Astaloy Mo in terms of local composition. In other words, a bainitic microstructure (similar to Astaloy Mo) is expected. Thus, in these areas it is more likely merely carbon which is causing the martensitic transformation to occur. Within the Distaloy DH specimens martensitic regions with approximately 4-5 wt. % of Cu were identified.

It can be summarized that the amount of bainite and martensite obtained for both materials is similar for the conditions of this study. This could be due to the following factors:

1) Nickel having lower diffusivity than copper contributing to higher inhomogeneity and Ni-rich regions

2) Nickel having higher hardenability than copper

3) Repelling effect between nickel and carbon.

Mechanical Properties

The results from the tensile testing, Figure 15, suggested that Astaloy Mo had significantly lower values for tensile strength and yield strength. But the elongation was reported to be higher when compared to Distaloy DC and Distaloy DH. This is due to a fully bainitic microstructure in the former and the presence of martensite and bainite in the microstructure for the latter. The average values of UTS and proof stress were higher for DH in comparison with Distaloy DC at both carbon levels.

With an increase in carbon content, slight increase in yield strength was observed for both Distaloy DC and Distaloy DH, since the amount of martensite in the microstructure increases. The tensile strength for both the materials did not increase with an increase in carbon content, since it is associated with a decrease in elongation. The elongation was slightly higher for DH at both the carbon levels, which might be due to the better homogeneity achieved by alloying Cu in contrast to Ni. The decrease in elongation with increase in carbon content could be because of the increase in the brittleness of martensite making the materials more brittle.

Astaloy Mo had the lowest value for apparent hardness among the materials because of its bainitic microstructure. Distaloy DC had a slightly higher apparent hardness values than DH at lower carbon level, but at the higher carbon level the values were similar, see Figure 16. This is because the microhardness values for martensite in Distaloy DC at lower carbon content were higher than that for DH. Also with an increase in carbon content, the martensite hardness increased for DH but remained similar for Distaloy DC, see Figure 16. Since the amount of phases were similar these two effects might be responsible for the trend observed.

Microhardness testing results indicated that the bainite hardness was similar for all the alloys, since the local composition for the bainitic regions in Distaloy DC and Distaloy DH are comparable to Astaloy Mo,

as discussed previously. Bainite average hardness increased for Distaloy DC with an increase in carbon content but not for the case of DH, see Figure 17. While the hardness values for martensite in Distaloy DC was higher than that for Distaloy DH at lower carbon content, at higher carbon level the martensite hardness is similar for both materials. With an increase in carbon content martensite hardness increased significantly for DH but the value remained similar for Distaloy DC. High microhardness value for martensite at lower carbon level (0.55wt. %) in Distaloy DC is most likely due to carbon repulsion effect of Ni-rich regions, discussed previously in the distribution of alloying elements section. In other words, Ni-rich regions cause a chemical potential gradient and thereby, uphill diffusion of carbon. Thus, the observed higher hardness of the martensite phase in Distaloy DC+0.55 wt. %C as compared to Distaloy DH+0.55 wt. %C is expected to be associated with the uphill diffusion of carbon

The heterogeneity of the microstructure of the Distaloy materials could be clearly seen from the microhardness profiles, see Figure 18. In contrast, the Astaloy Mo hardness profile indicates a homogenous microstructure. The reason for the mentioned discrepancy is related to the alloying methods used, which is via diffusion bonding in Distaloy grades and prealloying in Astaloy Mo. No carburization or decarburization effects could be observed since there is no hardness gradient between the surface and the core. Residual stress measurements (Table 3) showed that Astaloy Mo was the only material showing compressive surface residual stresses. The magnitude of the stress was not profound for the Distaloy materials but it was tensile. The carbon content did not show any considerable effect on the residual stresses. For the creation of residual stresses there should either be a cooling rate gradient between the surface and centre and/or a compositional gradient in which case the martensitic transformation occurs at different times/temperatures at the surface or the core, hence, inducing a residual stress state. Regarding the diffusion bonded powders, compositional heterogeneity exists inherently and different portions of the sample undergo transformations at different temperatures. The presence of pores or softer phases like the Ni-rich phases might also contribute to relieving the internal stresses. The metallographic investigations and the microhardness profiles did not indicate any sign of carburization or decarburization; and for the cross sectional area and the dimensions of the tensile specimen used, cooling rate gradient is not expected.

Porosity Analysis

PSF versus pore area plots were constructed to compliment and summarize prior mentioned findings from porosity analysis, see Figure 21. It could be deduced that the PSF values were similar for all the materials for a certain range in pore area which means that pores within similar size range had similar PSF values (irregularity). For all the materials, pores corresponding to an area range below 10 μm^2, the corresponding PSF values were close to 1. With an increase in pore area, the average PSF value decreased i.e., irregularity increased.

The current results are in agreement with previous studies which suggested that Astaloy Mo, Distaloy DC and Distaloy DH offered negligible differences in pore shape factor distribution implying that they present similar *physical* response to sintering, within the experimental conditions [26,32,39]. It should also be noted that the PSF measurements according to equation 4 are very sensitive to small irregularities but almost insensitive to small elongation Pores with larger size were associated with larger deviations from roundness and moreover, the largest size of pores is of importance since they

significantly affect mechanical properties, especially at lower densities [39].For the largest pore size measured (i.e. 1000-10000 μm^2), Distaloy DC with higher carbon content had higher volume fraction of pores than the rest(Figure 19). Despite the fact that the volume fraction of pores within the aforementioned range of size is less than 5 vol. %, these pores might have a significant impact in deteriorating the mechanical properties. However, for a complete understanding of pore morphology, along with PSF and pore area measurements, another shape factor has to be considered i.e., Fshape= Dmin/Dmax, Dmax and Dmin corresponding to maximum and minimum *Feret* diameters measured for the pore [40].

CONCLUSIONS

- Microstructural analysis of the samples sintered at 1120 °C and cooled with 2.5 °C/s revealed a fully bainitic microstructure for Astaloy Mo+0.55wt.%C while the structure was bainitic-martensitic for Distaloy DC and Distaloy DH at both carbon levels(i.e., 0.55 wt.% and 0.7 wt.%). Microstructure for Distaloy DC also consisted of Ni-rich areas due to the low diffusivity of Ni in Fe and these areas were identified to be austenitic based on the microhardness values and the Ni concentration.
- With an increase in graphite content the amount of martensite increased and bainite decreased for both Distaloy DC and Distaloy DH. The amount of phases obtained was approximately similar for both materials.
- Regarding tensile properties, DH was slightly better than Distaloy DC in terms of both tensile and yield strengths. Increase in graphite content from 0.55 wt. % to 0.7 wt. % did not increase neither the yield nor the tensile strength and only caused a decrease in elongation Astaloy Mo however, had the lowest strength values and highest elongation because of its completely bainitic microstructure.
- Apparent hardness values indicated that at lower carbon content (0.55 wt. %C) Distaloy DC had slightly higher values but at higher carbon level (0.7wt.%) both had similar values. This was in accordance with the microhardness values measured for the martensite phase in Distaloy DC and Distaloy DH.
- Within the microstructure for Distaloy DC and Distaloy DH bainitic areas did not contain any diffusion bonded alloying elements. Ni has lower diffusivity compared to Cu. However, if assuming a homogeneous distribution of Ni, the simulation results indicated that Ni promotes hardenability better than Cu. Molybdenum was however uniformly distributed within the microstructure owing to its prealloyed nature.
- Microhardness profiles did not indicate any carburizing or decarburizing effects within the materials but they reflected the heterogeneous microstructure of the Distaloy powders in contrast to a homogeneous microstructure of the Astaloy Mo.
- Astaloy Mo was seen to have compressive residual surface stresses while the Distaloy materials exhibited a slight tensile stress at the surface.

FUTURE WORK

- For further understanding of the benefits of the sinter hardening process, the results obtained from this project (i.e. sinter hardening) of the investigated alloys could be compared with the results obtained after the quench and tempering treatment
- The effect of the presence of nickel rich areas on the mechanical properties and the microstructure (in terms of carbon repelling effect) could provide more insight. For this purpose Distaloy DC grade should be sintered at higher temperatures and/or longer times for a more homogeneous distribution of Ni. The results should be compared with the current results to see the impact of more homogeneous distribution of Ni.
- For a better understanding of the effect of alloying elements, their diffusion behavior during different stages of sintering and the ability to promote hardenability should be understood for better tailoring of the alloys. Investigation of the materials at varying densities, sintering conditions and cooling rates for their microstructure would enable a better estimation of the benefit attained from the alloying individual alloying elements.
- Studies on dimensional control for these alloys should be conducted since it is an important factor in production of sintered components. This is also a factor that favors the usage of nickel against copper since the latter contributes to dimensional increase.
- Carbon content assessment would enable investigation concerning the repelling effect of carbon and nickel and also the carburization and decarburization effects along the cross-section of the samples.
- The reason for compressive residual stresses in Astaloy Mo, consistency and robustness in surface residual stress measurements results, should be analyzed and consequently comprehended.
- Fractography studies would provide useful information regarding the mechanical behavior of the materials.
- Precipitation effect in alloys containing Cu because of its low diffusivity in the ferritic microstructure could be studied with regard to evolution of phases during heat treatment.
- Redistribution of alloying elements during bainitic transformation in continuous cooling of P/M steels could be carried out.

References

1. **V.Lenel, Fritz.** *Powder Metallurgy- Principles and Applications.* Princeton, New Jersy : Metal Powder Industries Federation, 1980. 0918404-48-7.

2. *Improvements to Ferrous powders.* **G.F.Bocchini.** s.l. : Metal Powder Report, 1992, Vol. 48.

3. *A Review of Current Sinter Hardening Technology.* **Michael L.Marucci, George Fillari, Patrick King, and K.S.Narasimhan.** CInnaminson, NJ : Hoeganaes Corporation.

4. **Ferguson, Howard.** *Heat treatment of ferrous P/M parts,Powder Metal Technologies and Applications,Vol 7.* s.l. : ASM International Handbook, 2002.

5. **E.Totten, George.** *Steel Heat Treatment Metallurgy and Technologies.* s.l. : CRC Press,Taylor& Francis Group, 2007.

6. *Effect of materials and processing parameters on the microstrucutre and properties of sinterhardening alloys.* **G.L´Esperance, E.Duchesne and A.de Rege.** s.l. : Advances in Powder Metallurgy& Particulate Materials, 1996, Vols. Volume 3-11,Pg-397.

7. **Hoganas-3.** *Design and Mechanical Properties.* s.l. : Hoganas Handbook for Sintered Components, 2004.

8. *Effect of post sintering cooling rate on the properties of diffusion bonded steel materials.* **Tremblay, F.Chagon and Linda.** s.l. : European Powder Metallurgy Association, 2004.

9. *Lower Mo steels for high performance Powder Metallurgy applications.* **P.King, S.Patel, S.Shah, J.F Alleur, G.Wewers.** San Diego,California : International Conference on Powder Metallurgy and Particulate Materials, 2006.

10. *Achievable properties after different heat treatments of PM steels.* **Bjorn Lindquist, Sven Bengtsson,Sigurd Berg.** Sweden : Hoeganas AB.

11. *Properties and microstructure of PM materials prealloyed with Ni, Mo and Cr.* **Barbara Maroli, Sigurd Berg,Jeanette Lewenhagen.** s.l. : Hoganas,AB, Hoganas AB.

12. **P.Haasen, R.W.Cahn and.** *Physical Metallurgy.* Amsterdam : Elsevier Science Publisher, 1983.

13. **Krauss, George.** *Steels: Processing, Structure and Performance.* Ohio : ASM International , 2005. 0-87170-817-5.

14. **Avner, Sidney H.** *Introduction to Physical Metallurgy.* New York : Tata McGraw Hill, 1997.

15. *Controlling Hardenability of P/M steels.* **Lindskog, Per.** 26, s.l. : Powder Metallurgy , 1970, Vol. 13.

16. *Study of reduction/oxidation processes in Cr-Mo prealloyed steels during sintering by continuous atmosphere monitoring.* **E.Hryha, et al.** 4. pp.181-197, s.l. : Powder Metallurgy Progress, 2007, Vol. 7.

17. **Höganas-2.** *Production of Sintered Components-Handbook.* s.l. : Höganas AB, 2004.

18. *Powder Metallurgy Science, Page-380 to 390.* **M.German, Randall.** Princeton : Metal Powder Industries Federation, 1994.

19. *An Investigation into the effect of copper and graphite additions to Sinterhardened steels.* **C.Baran, Thomas F.Murphy and Michael.** NJ : Hoeganaes Corporation.

20. *Dimensional Control in Cu-Ni containing Ferrous PM Alloys.* **Murphy, Bruce Lindsley and Thomas.** Cinnaminson,NJ : Hoeganaes Corporation.

21. *Improved distribution of nickel and carbon in sintered steels through addition of chromium and molybdenum.* **M.W.Wu, K.S.Hwang and K.H.Chuang.** 2, s.l. : Powder Metallurgy , 2008, Vol. 51.

22. *Mechanical properties and dimensionals tability obtained with different alloying techniques.* **Larsson, Mats.** Höganäs,Sweden : Höganäs AB.

23. *Effect of post sintering thermal treatments on dimensional precision and mechanical properties in sinter hardened PM steels.* **Murphy, Bruce Lindsley and Thomas.** NJ : Hoeganaes Corporation .

24. **R.E.Reed-Hill.** *Physical Metallurgy Principles, Pg no.506-517.* Boston : PWS-Kent Publishing, 1973.

25. *Dimensional precision in sinter-hardened steels.* **Bruce Lindsey, Thomas Murphy.** s.l. : Hoeganas Corporation.

26. *Microstructural and mechanical characterisation of some sinterhardening alloys and comparisons with heat treated PM steels.* **G.F.Bocchini, B.Rivolta, G.Silva, E.Poggio, M.R.Pinasco and M.G.Ienco.** 4, s.l. : Powder Metallurgy, 2004, Vol. 47.

27. *Influence of chemical composition and Austenizing temperature on Hardenability of PM steels.* **A.Lindsley, Peter K.Sokolowski and Bruce.** NJ : Hoeganaes Corporation Cinnaminson.

28. **Höganäs.** *Höganäs Iron and Steel Powders for Sintered Components-Handbook.* s.l. : Höganäs AB, 2002.

29. *Evaluation of sinter hardening of different PM materials.* **Engström, Ulf.** s.l. : Höganäs AB, Sweden.

30. *Effect of sintering time and cooling rate on sinterhardenable materials.* **Ingalill Nyberg, Mary Schmidt and Peter Thorne,Jason Gabler, Thomas J.Jesberger and Stephen Feldbauer.** s.l. : Höganäs Inc and ABBOTT Furnace Co.

31. **G.Totten, M.Howes, T.Inoue.** *Handbook of residual stresses and deformation of steel.* Ohio : ASM International , 2002.

32. *Influence of Cooling rate on microstructural and mechanical porperties of alloys from diffusion-bonded powders, sintered in different conditions.* **Gian FIlippo Bocchini, Barbara RIvolta, Giuseppe Silva,**

Paolo Piccardo, Maria ROsa Pinasco, Eleonora Poggio. 4, pp.16-21, s.l. : P/M Science& Technology Briefs, 2002, Vol. 4.

33. **L.Wojnar, K.J.Kurzydlowskiand J.Szala.** *Quantitative Image Analysis -Page 403-427.* s.l. : ASM Handbook, ASM International, 2004.

34. **S.Prevey, Paul.** *X-Ray Diffraction Residual Stress Techniques, ASM Handbook Volume 10, Materials Characterization.* s.l. : ASM International .

35. **J.A:Pineault, M.Belassel and M.E.Brauss.** *X Ray Diffraction Theory and Residual Stress Measurement, ASM Handbook Volume 11.* s.l. : ASM International .

36. *Identification of Crack Initiation Sites of Ni-Containing Steels and Methods for Property Improvement.* **M.W.Wu, K.S.Hwang.** SanDiego, California : Advances in Powder Metallurgy and Particulate Materials, 2006.

37. *The Distribution of Substitutional Alloying Elements during Bainite Transformation.* **I Stark, G D W Smith and H K D H Bhadeshia.** 837, s.l. : Metallurgical Transactions A, April 1990, Vol. 21A.

38. **Shane Para, Lehigh University.** *Spinodal Transformation Structures, Vol.9, Metallography and Microstructures,ASM Handbook.* s.l. : ASM International, 2004.

39. *Microstructure and mechanical behaviour of porus sintered steels.* **N.Chawla, X.Deng.** s.l. : Materials Science and Engineering A, 98-112, 2005, Vol. 390.

40. *Image analysis investigation of the effect of porcess variables on the porosity of sintered chromium steels.* **T.Marcu Puscas, M.Signorini, A.Molinari, G.Straffelini.** 1, University of Trento : Materials Characterization, 2003, Vol. 50.

41. **Hoganas.** *Design and Processing of Powdered Steels.* s.l. : Hoganas Iron and Steel Powders for Sintered Components.

42. *Performance of Sinter hardened P/M steels.* **Barbara Maroli, Sigurd Berg, Mats Larsson, Ingrid Hauer.** s.l. : Hoganas, Sweden.

43. *Influence of controlled atmospheres on the proper sintering of carbon steels.* **Bocchini, G.F.** 1, s.l. : Powder Metallurgy Progress, 2004, Vol. 4.

44. *Effect of post-sintering cooling rate on properties of diffusion bonded steel materials.* **F.Chagnon, Linda Tremblay.** s.l. : EPMA Conference, 2004.